On the network orientational affinity assumption in polymers and the micro-macro connection through the chain stretch

Víctor Jesús Amores[a], Khanh Nguyen[a], Francisco Javier Montáns[a,b,*]

[a] *E.T.S. de Ingeniería Aeronáutica y del Espacio. Universidad Politécnica de Madrid, Pza. Cardenal Cisneros 3, 28040-Madrid, Spain.*
[b] *Dept. of Mechanical and Aerospace Engineering. Herbert Wertheim College of Engineering, University of Florida, Gainesville, FL 32611, USA*

Abstract

We question the network affinity assumption in modeling chain orientations under polymer deformations, and the use of the stretch measure projected from the right Cauchy-Green deformation tensor (or non-affine micro-stretches derived from that measure) as a basic state variable for the micro-macro transition. These ingredients are standard, taken from the statistical theory of polymers, and used in most micromechanical polymer network and soft tissue models.

This assumption imposes a constraint in the network which results in an anisotropic distribution of the orientation of the chains and, hence, in an additional configurational entropy that should be included. This additional entropy would result in an additional stress tensor. But an arguably more natural alternative, in line with the typical assumption for the chain behavior itself and with the disregard of these forces, is to consider that the network may fluctuate unconstrained to adapt to macroscopic deformations. This way, the isotropic statistical distribution of the orientation of the chains is maintained unconstrained during deformation and no additional stress is imposed. We show that this free-fluctuating network assumption is equivalent to consider the stretch projected from the stretch tensor (instead of the right Cauchy-Green deformation tensor) as the state variable for the deformation of the network chains.

Employing our recent data-driven macro-micro-macro approach, we show very important differences in predictions using both assumed behaviors, and demonstrate that with the free-fluctuating network assumption, we can obtain accurate predictions for all tests in polymers using just one test curve to calibrate the model. With the same macro-micro-macro approach employing the network affinity assumption, we are capable of capturing accurately only the test used for calibration of the model, but not the overall polymer behavior. Further numerical examples are developed to give supporting evidence for the unconstrained orientation assumption.

Keywords: Polymers; Affine deformations; Chain models; Hyperelasticity; Soft materials; Entropy

1. Introduction

Polymers have an intrinsic entropic nature (see e.g. Sec. IV in Anthony et al. (1942), Fig. 2.8 in Treloar (1975) and Gusev and Schwarz (2019)), meaning that they are formed of interconnected networks of large chains which vibrate freely and, statistically, produce forces, nonvanishing in average, when such movement is constrained by a given continuum deformation (Flory, 1969; Ward and Hadley, 1993; Argon, 2013; Mark and Erman, 1988). This entropic nature results in the characteristic soft behavior, to which the internal energy plays only a minor role in the intramolecular interactions (Flory, 1969; Treloar, 1975, Ch.13). The practical and accurate modelling of polymers has been a very complex task which involved many researchers during the last century, resulting in a number of models "approximately equal to the number of researchers

*Corresponding author, e-mail: fco.montans@upm.es

who work (or worked) in the field" Volokh (2016). In essence, the two main approaches to model the stress-strain behavior of polymers are the phenomenological approach and the micromechanical approach.

Even though there are earlier works, the phenomenological Mooney (1940) model is probably the first model to give a relevant correlation to several types of tests at moderate stretches. Furthermore, the simplest form including only the first invariant I_1 of the Cauchy-Green deformation tensor $\boldsymbol{C}$, is coincident with the Gaussian micromechanical *affine* approach, and it is well-known as the Neo-Hookean model. However, Mooney, and later many other authors (Rivlin, 1948; Rivlin and Saunders, 1951; Hart-Smith, 1966; Yeoh, 1993; Yeoh and Fleming, 1997; Horgan and Saccomandi, 2002; Kroon, 2011; Kiêm and Itskov, 2016, among others), already noted the need to include the second invariant I_2 of $\boldsymbol{C}$ in the stored energy function for capturing well several deformation modes, an issue often referred to as *"small deviations from the statistical theory"* (Claim C0) (Yeoh and Fleming, 1997; Treloar, 1975, Sec. 10.8). This *deviation*, which is related to a term in I_2, was made apparent by Mooney in his "Mooney plots", in which experiments in polymers consistently exhibited a slope not predicted by the classical statistical theory. This was further analyzed by Rivlin and Saunders (1951) and Obata et al. (1970). However, "in contrast to the original success of the statistical theory, the failure to secure any very significant understanding of the relatively rather small deviations from the theory, despite repeated attempts over a period of 30 years [now 75], is disappointing" (Treloar, 1975, p.229). Nonetheless, Mooney-Rivlin approaches, including the I_2 term, are commonly used in finite element codes because of their practical fitting capability. A phenomenological alternative to the Mooney-Rivlin invariants (or other similar alternative invariants, Criscione (2003), Shariff (2017)) are models based on principal stretches, specially those using the Valanis and Landel (1967) decomposition. Two well-known models of this type are those from Ogden (1972) and Shariff (2000). Remarkably, these models are known to perform very well in polymers, specially when they are characterized from several test types (Ogden et al., 2004; Markmann and Verron, 2006; Kiêm and Itskov, 2016). Indeed, Ogden's model is also very common in finite element codes and a frequent choice by engineering modelers.

The micromechanical theory starts probably with the work of Staudinger (1920), who recognized the polymer long chain structure and coined the word *macromolecule*. It was followed by the understanding of polymers through the kinetic/entropic theory of reversible deformations (Sec. 6 in Meyer et al. (1932)) and by the treatment of polymers as free joint chains in Kuhn (1934, 1936); Kuhn and Grün (1942); the latter introducing the non-Gaussian distribution. The statistical distribution of chain lengths and the stress-strain relation, were given by Wall (1942). The non-Gaussian stress-strain relation based on the Langevin function was given by James and Guth (1943), who also introduced the three-chain model. James and Guth (1943) further addressed in an appendix a problem relevant to the micro-macro transition in polymer networks: *the affinity in displacements of junction points* of the network. They made a mathematical study assuming a Gaussian approach and that the joints at the boundary are fixed, whereas the rest of the junction points are free to fluctuate with the network around an equilibrium position. The conclusion of this early study is discussed and summarized in Sec. 4.7 of Treloar (1975): junction points (their statistical equilibrium position) move in average in a pattern affine with (as attached to) the continuum, and the loads over the junction points are just those from the chains. Hence, at least in the Gaussian (moderate stretches) domain, this finding supports the computation of the chain stretch λ_{ch} from the continuum deformation gradient, just projecting $\boldsymbol{C}$ on the original end-to-end direction of the chain. Since then, this is the approach followed by most works (Treloar (1975); Ward and Hadley (1993); Holzapfel (2000); Volokh (2016)). Furthermore, Flory and Rehner (1943) developed a non-affine four-chain model. The chains connected the vertices of a representative tetrahedron cell with a central point. The junction points at the vertices followed affine displacements, but the central point moved freely as to maximize the entropy of the system. Their conclusion was again that the non-affine movement of the central point had little contribution to the entropy of the Gaussian model. But Treloar used an evolution of this model to the non-Gaussian domain (large stretches) and compared the average chain tension for the affine and non-affine cases. He observed that the upturn of the tension-stretch curve moved considerably to large stretches for the non-affine case when compared to the affine one, delaying chain locking effects and producing large discrepancies in the chain tensions in that part of the domain; see Fig. 6.10 in Treloar (1975) and therein references. Importantly, this work showed that, whereas the affinity assumption seemed not to affect substantially predictions at low-to-moderate stretches, it may be overconstraining the models at moderate-to-large stretches.

Flory (1976) (see also therein references) questioned the distinction between "free" junction points and *macroscopic* constraints fixing *microscopic* junction points (in essence, macroscopic entities which fix the microscopic ones that themselves constitute the macroscopic entities). In consequence he further developed the phantom network model, which however just resulted in a modification of the constant leading the first invariant, see Eq. (40) in Flory (1976). A more detailed treatment of the phantom network theory was introduced by Flory and Erman (1982) adding a term accounting for the constraints, no longer proportional to the first invariant of $\boldsymbol{C}$, but still based on the Gaussian framework. Indeed this later improvement has been introduced in the 8-chain model to better capture the low stretches behavior by including I_2-like effects (Arruda and Boyce, 2000, Fig. 6), yet at the cost of introducing two additional fitting parameters. But the original Arruda and Boyce (1993) 8-chain model is one of the most successful models precisely because it has only two parameters which can be obtained from a single test. The model may be considered as affine because it consists of 8 chains in the diagonals of a cube with sides oriented towards the principal stretches, with the central joint point conceptually allowed to move freely, but subject to the symmetry of the cell (all chains get the same stretch). Cube vertices move affinely with the continuum and, as previous micromechanical affine models, the strain energy only depends on the first invariant. However, deformations in the 8 chains just represent average deformations of the chains in all directions, so it may also be considered conceptually a non-affine model (Arruda and Boyce, 2000; Miehe et al., 2004) with a "single non-affine network stretch $\lambda = \sqrt{I_1/3}$" as *micro-macro* transition (Miehe et al., 2004). Indeed, this "non-affinity" of the Arruda and Boyce (1993) model is highlighted as a possible reason behind the success of this model when compared to the well-known but *"somewhat surprising lack of success of the full network model"* (Claim C1) (Arruda and Boyce, 2000, p.509). The (affine) full network model ("micro-sphere" or "complete assembly of chains") was developed by Treloar and co-workers, among others; see Treloar (1975) and therein references. It is an attractive idea for current computational power so it has been extended to soft tissues (e.g. Alastrué et al. (2009); Sáez et al. (2012); Menzel and Waffenschmidt (2009); Waffenschmidt et al. (2012)). But the performance of the affine version motivated the Miehe et al. (2004) remark that *"it is a well-known fact that the* [chain stretch] *affinity assumption yields a model response that is not in agreement with experimental observations, in particular in the range of large deformations"* (Claim C2); see also Wu and van der Giessen (1993). This claim is in line with the commented previous findings by Treloar.

To overcome the deficiencies of the affinity assumption, more complex models have been introduced which aimed to: (1) correct the affine deformation of the surface (weight) associated to the chain during deformations (motivated on slip links or forest chains and with a practical effect that may be equivalent to include the second invariant in phenomenological models, cf. Eq. (22) in Kiêm and Itskov (2016), Eq. (14) in Kroon (2011)); (2) correct the affine chain stretch obtained from the continuum right Cauchy-Green deformation tensor (a similar effect as to include fluctuating junction points, inhomogeneous subnetworks or fluctuating micromechanical fields, cf. Eqs. (14) and (17) of Kiêm and Itskov (2016), Eq. (11) in Kroon (2011)). The first issue is addressed by tube models (Edwards, 1967; Edwards and Vilgis, 1988; Kaliske and Heinrich, 1999; Qin et al., 2012). Their probability density function and energy in terms of tube diameter can be found in Doi and Edwards (1988). The second issue has been addressed with non-affine stretches (Rubinstein and Panyukov, 1997; Miehe et al., 2004; Lang, 2017). The non-affine microsphere model (Miehe et al., 2004) has all these ingredients (non-affine tube and non-affine chain stretch) to capture all deformation modes at both moderate and large stretches. Other models based on the same or similar ideas have been recently proposed (Kroon, 2011; Lopez-Pamies, 2010; Kiêm and Itskov, 2016; Verron and Gros, 2017; Xiang et al., 2018), which add to classical alternatives as the slip-link (entanglements) model (Ball et al., 1981). Other mixed models include similar improvements as, e.g. including I_2 dependency in the Gent (1996) model by Horgan and Saccomandi (2002); Horgan and Schwartz (2005).

In summary, all the improvements on the basic Mooney and Gaussian models have been developed with the purpose of better capturing the experimentally observed mechanical behavior. Conclusions respect to micromechanics assumptions have been derived from the improved predictive power under different deformation modes when such assumptions are considered versus when they are not. In this regard, there are several papers in which the predictive power of different models is assessed; the works of Steinmann et al. (2012) and Markmann and Verron (2006) (to which the predictions from Bergström (2015) for Treloar's tests and Kiêm and Itskov (2016) for Kawabata et al. (1981) tests can be added) are excellent summaries, and of

special interest to understand the state of the art in this respect. Steinmann et al. (2012) show predictive capabilities of 13 models respect to Treloar's data, with special attention when only one test is employed in the characterization and thereafter the model is employed to predict other tests. Except for the 8-chain model and the Carroll (2011) model (who puts emphasis again in the relevance of the second invariant to capture different test modes), predictions for other tests not employed to fit the material parameters, are deficient, including those of the affine microsphere or full network model (see C1 above). Motivated on the observation that *"it is now well-established that a unique experiment is not sufficient to characterize a rubber-like material even assuming that it is elastic"* (Claim C3), Markmann and Verron (2006) focused on the overall predictive power of 20 models when experimental data from several tests are employed simultaneously in the characterization. Markmann and Verron (2006) used a complex fitting procedure, using simultaneously gradient and genetic algorithms and different test weightings when needed for achieving best fits. Furthermore, both the Treloar (1944) and Kawabata et al. (1981) data were employed. The Kawabata et al. (1981) experiments, on a similar material than that used by Treloar (1944), are considered "a very tough" benchmark (Kiêm and Itskov, 2016) because only three models (four including Kiêm and Itskov (2016)) are known to capture both experimental sets with the same material parameters. In particular, the Kawabata et al. (1981) tests comprise all possible deformation states for an incompressible material within the tested experimental ranges.

Whereas conceptually one would expect some practical modelling benefit from the detailed micromechanical approach (i.e. less tests as in the Arruda and Boyce (1993) model), until Amores et al. (2020) no material model has been capable of fitting the Kawabata et al. (1981) experiments, or similar ones, using only one test curve. Remarkably, the phenomenological Ogden (1972) (Fig. 3 in Markmann and Verron (2006)) and the Shariff (2000) (Fig. 13 in Kiêm and Itskov (2016)) models perform as well as complex non-affine micromechanical models (Figs. 4, 11 and 12 in Kiêm and Itskov (2016)). Also remarkably, the constrained junctions model (based on the non-affine "free joints" phantom network), behaved very well in its Gaussian domain (cf. Fig 5 in Markmann and Verron (2006))

Despite (and in view of) all the previous comments, we see a paradoxical duality in the micromechanical models which, as commented, has also concerned many authors in the past, motivating models like the phantom network model or the slip-link model. On one hand, chains are considered fully within the statistical entropic approach, with links free to fluctuate (maybe "tube-constrained" by forest chains), but junctions are assumed fixed to the continuum (the affinity assumption), somehow mixing an entropic view for chains with a more conventional view for the network structure. The practical implications relate to the use of affine chain representative weights and the use of an affine stretch from the Cauchy-Green deformation tensor. These lead to the mentioned unsatisfactory results, and to the several theories of increasing complexity to correct both aspects of the affinity assumption, both regarding a modified assigned surface (tube diameter) and a modified affine stretch of the type $\Lambda^{q/2}$, where Λ is the squared stretch from the projection of $\boldsymbol{C}$ in the chain direction. There is experimental evidence in collagenous tissues and polymer hydrogels that rotations may be non-affine (e.g. Wen et al. (2012); Gilbert et al. (2006); Billiar and Sacks (1997) and therein references). However, we are not aware of any attempt to treat the network itself in the same entropic way as the chains; i.e. to consider that chains may orientate randomly in the network (the orientations as statistical values), and that a change in their original angular distribution should be related to a nonvanishing work-conjugate generalized force of entropic origin.

Noteworthy, in the statistical theory, the chain length itself results to be not relevant in the chain behavior: only the chain stretch and the possible number of microstates (which in the unconstrained theory is related to the orientational distribution of links) play a role in the chain tension. If the network itself is allowed to fluctuate, and the chains within that network are allowed to adapt their direction to maximize entropy, there is an additional configurational entropy associated to the relative orientation of the chains. For example all chains oriented towards the same direction have much less entropy than an isotropic statistical distribution of chains (the distribution accepted in the undeformed configuration). The free reorientation of chains seems to us natural because, in fact, the chain itself has no defined "orientation": the end-to-end vector $\boldsymbol{r}$ is just the links average direction (r is the constraint for the links angular distribution). Then, we see the "chain direction" not as a fixed end-to-end vector of a particular chain, but as a dummy variable to account for the chains (or chain segments) statistically oriented towards that direction. This is conceptually

similar to moving the plunger in a gas container: the velocity vector distribution of the particles remains isotropic at equilibrium. The chain behavior would just depend on the available configurations which do not only depend on the average number of links between joints, but also on other constraints affecting the chain extension (e.g. forest chains). The change in orientational density of chains (direction representative weight) would be tied to a respective change of the network configurational entropy and to a related generalized force (stress). We assume that this generalized force may be neglected in most cases (it vanishes or is small statistically, at least whereas the chains entropy does not drop sufficiently), resulting in a non-affine model respect to the chains orientation. This non-affinity is just related to the preservation of the isotropy (maximum entropy) in that orientational density, but chain stretches remain otherwise affine under this assumption.

Of course this theory may (should) be seen as a questionable theory; so in this paper we *do* question it. As Heinrich et al. (2003) noted, "it is not unusual for people to reconsider issues that almost everyone else in a field considers well established [...]. This is a useful endeavor [...] but [...] the results must demonstrate improvements over the models to be replaced". The proposed theory questions the widely adopted affine chain orientations distribution, and along it the widely accepted claims (C0), (C1), (C2) and (C3) above, which are ubiquitous in the field. These are based on previous experience by many authors, and that we also felt unquestionable until the findings herein reported. Then, the first step must be to demonstrate that the assumption results in improvements over those well established theories. In Amores et al. (2020) we developed a macro-micro-macro (MMM) approach to model polymers. Based on these assumptions, the approach performs a reverse-engineering of the average chain behavior from a *single* macroscopic test curve (*any* type of test which has a sufficient stretch range) (contradicting C3). This function embeds all effects in the longitudinal chain behavior (mean number of configurations due to links, entanglements and other constraints), but uses an affine stretch if chain orientations are considered to remain isotropic (contradicting C2). We have shown in Amores et al. (2020) that the chain function, reverse-engineered from a single test curve, reproduces to excellent accuracy (better than the above-mentioned models) all the true biaxial cases from Kawabata et al. (1981) via angular integration , including low and large stretch ranges, and both tension axes. The method uses the WYPiWYG approach (Crespo et al., 2017; Latorre and Montáns, 2014; Romero et al., 2017; Latorre et al., 2017b; Crespo and Montáns, 2019) to determine the chain function just solving a linear system of equations (i.e. no classical material parameters or nonlinear optimization procedures: this is a quasi-automatic procedure). Moreover, the reverse-engineered chain function is essentially the same using any test curve on the material to calibrate the model; see discussion in Amores et al. (2020), where we also report a comparison of predictions with the chain function obtained from Treloar's tests. We also show therein that the model performs equally well in two types of silicones tested with a similar series of true biaxial tests by Kawamura et al. (2001). Hence, in practice, this very simple approach seems to outperform the most sophisticated models.

Then, the question we address in this paper is whether the predictive power of the MMM approach is just due to numerically reverse-engineer the chain function (so the performance could be attributed only to a better, phenomenological fit) or to the previous non-affine orientational assumption (more important, but which practical implementation is even simpler than that of the affine assumption because, e.g. it preserves the optimality of the integration rules in the sphere). Indeed, the MMM model is similar to a full network model, known to fail to provide good results employing an affine angular distribution of chains, but performing in an excellent manner (contradicting C1) if an unrestricted chains orientation distribution is assumed.

The rest of the paper is organized as follows. First, in Sec. 2 we recall basic facts as the Gibbs form of the entropy understood as a function of probability distributions, and the observation that if the system is unconstrained, entropy is maximized for the isotropic distribution. We then address the additivity of the entropy of a system made of subsystems (i.e. distributions of chains made themselves of distributions of links). We recall the orientational distribution of links in a chain to emphasize that the deviation from the statistical isotropic distribution (the chain constraint) is responsible for the tension in the chain. In consequence, we show that a non–isotropic distribution of chains in the network would result in an additional entropy (if we preserve the statistical view) with an associated additional stress. These are neglected in the affine deformations approach. To address the practical consequence of the different approaches, in Sec. 3

we show that whereas the homogenization of the affine deformation uses the micro-macro chain stretch connection from $\boldsymbol{C}$, the unconstrained chain orientational approach is accounted for just by employing a micro-macro chain stretch connection from $\boldsymbol{U} = \sqrt{\boldsymbol{C}}$. Since one may think that differences between both approaches should be modest (i.e. just using a chain stretch obtained from $\boldsymbol{C}$ or from $\boldsymbol{U}$ which are equal in principal directions), in Sec. 4 we address those differences using the same Neo-Hookean model but based on the different micro-stretches. Here we show that the non-affine Neo-Hookean-like model predicts the previously unexplained slope in Mooney plots related to the I_2 invariant (contradicting claim C0). Finally, in view of these differences, we asses in Sec. 5 the practical impact of considering both the affine chains orientation assumption and the unconstrained isotropic one to capture multiaxial behavior of real polymers. Several additional simulations are performed to give supporting evidence on the assumption. Whereas such evidence may be considered as nonconclusive because it is based on a specific full network approach, it may be one of the reasons why, despite of the above-mentioned efforts, no model has been capable of predicting the behavior of polymers using a single test curve to determine the material parameters; furthermore, they necessitated of non-afffine micro-stretch and micro-area corrections to predict that behavior even when using several tests simultaneously to obtain the material parameters.

We recommend to the reader interested mostly in the practical implications of this work to start with Secs. 4 and 5 (which can be read independently), then proceed to Sec. 3, and if interested in the theoretical motivation to address Sec. 2.

2. Entropy of chains and networks

2.1. Boltzmann entropy

The entropy of the system may be understood employing Boltzmann's theory following the principles of statistical mechanics. According to Boltzmann, the entropy S of a system may be computed from the quantity W of possible equivalent system states from microstates corresponding to that system macrostate

$$S = k_B \ln W \tag{1}$$

where k_B is Boltzmann's constant. The entropy may be considered as a measure of internal equilibrium in the system, or as a measure of homogeneity within the system. In general, if we have a system made of N components, and $i = 1, ..., n$ different microstates (slots), each microstate with N_i components such that $N = \sum_{i=1}^{n} N_i$, from the theory of combinatory, the number of possible equivalent states, is[1]

$$W = \binom{N}{N_1}\binom{N - N_1}{N_2}...\binom{N - \sum_{i=1}^{n-1} N_1}{N_n} = \frac{N!}{\prod_{i=1}^{n} N_i!} \tag{2}$$

where the number of possible different states is n^N. Hence, from Eq.(1), the entropy is

$$S = k_B \ln N! - k_B \sum_{i=1}^{n} \ln N_i! \tag{3}$$

For N_i sufficiently large, we can think of a continuous distribution so we can apply the Stirling approximation $\ln N! \approx N \ln N - N$. Using this approximation in Eq. (3) and considering the case of interest below such that $N = \sum_{i=1}^{n} N_i$, we have the Gibbs form of the entropy

$$S = k_B \left[N \ln N - \sum_{i=1}^{n} N_i \ln N_i \right] = -k_B N \sum_{i=1}^{n} \rho_i \ln \rho_i \tag{4}$$

[1]The actual original expression, that preserved additivity of the entropy in mixtures, does not contain $N!$, see Müller and Weiss (2005), Sec. 16.2, p. 171, but we keep the best known and intuitive expression for the discussion.

where $\rho_i = N_i/N$ is the *relative* density in the microstate (discrete distribution). Then taking $C = k_B N$, we can also write $S = -C\sum_{i=1}^{n} \rho_i \ln \rho_i$, and if the number of microstates n is large, we can take a distribution

$$S = -C \int_{\Theta} \rho(\theta) \ln \rho(\theta)\, d\theta \geq 0 \tag{5}$$

where Θ is the continuous domain of microstates and $\rho(\theta)$ is the continuous distribution. This last formula is connected to Shannon's entropy of information (in that case typically with a logarithm in base 2).

2.2. Unconstrained maximum entropy distribution

Assume that $\theta \in \Theta \equiv (\theta_1, \theta_2)$. The principle of maximum entropy states that at equilibrium

$$\rho(\theta) \text{ such that } S(\rho(\theta)) = -C \int_{\theta_1}^{\theta_2} \rho(\theta) \ln \rho(\theta)\, d\theta \to \max \tag{6}$$

meaning that the most probable $\rho(\theta)$ is such that a variation $\delta\rho(\theta)$ over it implies that there is no variation in the entropy, i.e. $\delta S(\delta\rho(\theta))\,|_{\rho(\theta)} = 0$ for all $\delta\rho(\theta)$. Computing the first variation of the term $\ln(\rho(\theta))\rho(\theta)$ we obtain $\delta\{\ln(\rho(\theta))\rho(\theta)\} = [1 + \ln(\rho(\theta))]\,\delta\rho(\theta)$ and the variation of the entropy functional is

$$\delta S(\delta(\theta)) = -C \int_{\theta_1}^{\theta_2} [1 + \ln(\rho(\theta))]\,\delta\rho(\theta)\, d\theta = 0 \tag{7}$$

From the definition of $\rho(\theta)$ (as the continuous version of N_i/N, a probability density), we must have

$$\int_{\theta_1}^{\theta_2} \rho(\theta)\, d\theta = 1 \;\Rightarrow\; \delta \int_{\theta_1}^{\theta_2} \rho(\theta)\, d\theta = \int_{\theta_1}^{\theta_2} \delta\rho(\theta)\, d\theta = 0 \tag{8}$$

However, the variation $\delta\rho(\theta)$ is arbitrary (e.g. may vanish in an arbitrary part of the domain), so in general Eqs. (7) and (8) must be fulfilled simultaneously in any arbitrary domain Θ^*. Hence $1 + \ln(\rho(\theta)) = \alpha$, constant for all θ, or equivalently $\rho(\theta)$ is the constant distribution, a well-known result, whose value must be $\rho(\theta) = 1/(\theta_2 - \theta_1)$ to comply with Eq. (8).

In summary, the principle of maximum entropy gives a uniform ("isotropic") distribution as the most probable distribution. Note that a similar conclusion is obtained from Eq. (4) if we consider N_i a continuous variable respect to which a derivative may be made

$$\frac{\partial S}{\partial N_i} = -k_B \left(\ln \frac{N_i}{N} + 1\right) = 0 \;\Rightarrow\; \rho_i = \frac{N_i}{N} = \tilde{C} \exp(-1) = \gamma \tag{9}$$

so all N_i and all ρ_i are equal and $\tilde{C}$,γ are constants obtained from the requirement that $\sum_i \rho_i = 1$ (which may also be introduced as a constraint). Note that if all N_i are in the same slot, the entropy is minimal (zero), and the maximum entropy, obtained for the isotropic distribution, is proportional to N.

2.3. Configurational entropy at two scales

In polymers we deal with long molecules modeled as chains, and we compute the entropy of the chains according to their possible random link configurations. But chains themselves form a network, and they may also orientate randomly in that network. If two subsystems (1) and (2), each with its own entropy are combined, but no configurational entropy of the combination is accounted for, the entropies are just summed up because each subsystem just adds slots (microstates) for their own components, totaling $n_1 + n_2$ slots. Because we assumed subsystems do not mix, the total combinations of the system are $N^{(1)}!N^{(2)}!$, i.e.

$$S = k_B \ln \frac{N^{(1)}!N^{(2)}!}{\prod_{i=1}^{n_1} N_i^{(1)}! \prod_{i=1}^{n_2} N_i^{(2)}!} = k_B \ln \frac{N^{(1)}!}{\prod_{i=1}^{n_1} N_i^{(1)}!} + \ln \frac{N^{(2)}!}{\prod_{i=1}^{n_2} N_i^{(2)}!} = S^{(1)} + S^{(2)} \tag{10}$$

Hence, in the literature the entropy of ensembles of chains is typically the sum of the entropies of the individual chains. However, when the subsystems themselves may also combine as systems, we are in practice adding a third "system", which in this example consists of two elements, namely (1) and (2), so say $N^{(3)}=2$. These subsystems may be placed in n_3 slots, so we have that the entropy of this new (3) system is $S^{(3)}=k_B\ln(N^{(3)}!/\prod_{i=1}^{n_3}N_i^{(3)}!)$.

In general, the total entropy of the ensemble consisting of Z subsystems, and one system labelled "$Z+1$" combining (but do no mixing) those subsystems is

$$S=k_B\ln\frac{\prod_{z=1}^{Z+1}N^{(z)}!}{\prod_{z=1}^{Z+1}\prod_{i=1}^{n_z}N_i^{(z)}!}=\sum_{z=1}^{Z+1}k_B\ln\frac{N^{(z)}!}{\prod_{i=1}^{n_z}N_i^{(z)}!}=S^{(Z+1)}+\sum_{z=1}^{Z}S^{(z)} \tag{11}$$

where $S^{(Z+1)}$ is the additional configurational entropy of the combination of immiscible subsystems. This entropy may be considered if chains orient statistically in the network. Of course, if Z is large, $S^{(Z+1)}$ may be neglected as long as $N^{(Z+1)}$ is in the same order as $N^{(z)}$, unless the entropies of the subsystems drop sufficiently so that of the system becomes dominant.

2.4. The entropy of a single chain

This statistical approach is typically employed to study the behavior of rubber-like materials considering that a rubber molecule can be understood as a chain compound of N independent random links, and the material as a cross-linked network of such chains. The changes in the internal energy U are neglected (cf. Fig. 8a in Anthony et al. (1942), Fig. 2.8 in Treloar (1975) or Fig. 6.3 of Argon (2013)) when compared to the possible changes in the entropic energy $-TS$, where T is the absolute temperature; i.e. the power in isothermal cases (as considered along this work) is $\dot{\Psi}=-T\dot{S}$. Then, the forces in the system $\mathfrak{f}$ are due to changes in its entropy $\mathfrak{f}(\bullet)=-T\partial S/\partial(\bullet)$, where $(\bullet)$ are the set of selected kinematic variables describing the change of entropy and $\mathfrak{f}(\bullet)$ are their work-conjugate generalized forces. The treatment of the chain entropy and related tension is well known, but it is presented here in terms of orientation of links to emphasize the trinomial "kinematic constraint $\Leftrightarrow$ biased-orientational-distribution $\Leftrightarrow$ generalized force", making a parallelism with that of the network itself as a system of chains.

The possible microstates for a link are its possible orientations in space. To make the reasoning simpler a discretization in the space of possible directions can be made. That way, the polar θ, and the azimuthal φ axis, which are continuous, are discretized with the values $\theta=\theta_1,\theta_2,\ldots,\theta_p$ and $\varphi=\varphi_1,\varphi_2,\ldots,\varphi_q$. With this approach, the space is represented by a grid with $p\times q$ possible combinations of the values (θ_i,φ_j). Let $N_{\theta_1\varphi_2}$ be the number of chains that share the spatial orientation defined by the polar angle θ_1 and the azimuthal angle φ_2. Boltzmann's entropy of the chain is

$$S_{ch}=k_B\ln W\quad\text{with}\quad W=\frac{N!}{\prod_{i=1}^{p}\prod_{j=1}^{q}N_{\theta_i\varphi_j}!} \tag{12}$$

Following the steps in Sec. 2.1, see Eq. (4), and defining the density $\rho(\theta_i,\varphi_j)=N_{\theta_i\varphi_j}/N$, we get

$$S_{ch}=k_B\ln W=-k_B\sum_{i,j=1}^{p,q}N_{\theta_i\varphi_i}\ln\left(\frac{N_{\theta_i\varphi_i}}{N}\right)=-k_BN\sum_{i,j=1}^{p,q}\rho(\theta_i,\varphi_j)\ln\rho(\theta_i,\varphi_j) \tag{13}$$

It is worth to note that if we split the chain into two chains, see Fig. 2, with equivalent distributions ($N^{(1)}=\alpha N$ and $N^{(2)}=(1-\alpha)N$ means $N^{(1)}_{\theta_i\varphi_i}=\alpha N_{\theta_i\varphi_i}$ and $N^{(2)}_{\theta_i\varphi_i}=(1-\alpha)N_{\theta_i\varphi_i}$), we have that the entropy of the system made from both chains is the same as that of the single chain; i.e. only the orientational distribution densities $\rho(\theta_i,\varphi_j)$ are relevant. For continuous distributions—see Eq. (5)

$$S_{ch}=-k_BN\int_\Omega\rho_{links}(\theta,\varphi)\ln\rho_{links}(\theta,\varphi)\,d\Omega \tag{14}$$

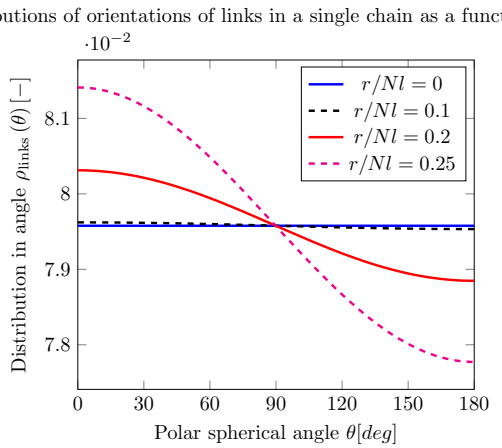

Figure 1: Distribution of the orientation of the links in a single chain as a function of the fractional extension r/Nl. The distribution is isotropic in the angle φ around the chain axis. In average, the links are oriented in direction $\boldsymbol{r}$.

where $d\Omega = \sin\theta d\theta d\varphi$ is the solid angle of the unit sphere (i.e. really the distribution must be taken per unit surface, not per angle aperture, so all slots are equal). The *unconstrained* distribution that complies with the maximum entropy is the constant distribution, see Sec. 2.2, i.e. $\rho_{links}(\theta,\varphi) = 1/\Omega = 1/(4\pi)$, which means that a given link has the same probability to be oriented at any given angle.

We now introduce a kinematic variable describing the macrostate and the constrained entropy of the chain. This variable is the end-to-end vector distance $\boldsymbol{r} = r\hat{\boldsymbol{r}}$, with modulus r and direction $\hat{\boldsymbol{r}}$. Then, we require that the projection of all links in the direction of $\boldsymbol{r}$ sum r. To maximize the entropy under this constraint, we generate the Lagrangean

$$L = -k_B \sum_{i,j=1}^{p,q} N_{\theta_i\varphi_j} \ln\left(\frac{N_{\theta_i\varphi_j}}{N}\right) + f_T\left(r - \sum_{i,j=1}^{p,q} N_{\theta_i\varphi_j} l\cos\theta_i\right) \tag{15}$$

where l is the 1D length of the link, θ is now the angle between the link and $\hat{\boldsymbol{r}}$ and f_T is the Lagrange multiplier (the force associated to the constraint). Then, from $\partial L/\partial N_{\theta_i\varphi_j} = 0$, normalizing $\sum \rho_{links}(\theta_i,\varphi_j) = 1$, we get — see Fig 1:

$$\rho_{links}(\theta_i,\varphi_j) = \frac{N_{\theta_i\varphi_j}}{N} = \frac{\exp(-\beta\cos\theta_i)}{\sum_{i,j=1}^{p,q}\exp(-\beta\cos\theta_i)} \tag{16}$$

with $\beta = f_T l/k_B$. Considering $N_{\theta_i\varphi_j} = \bar{C}N\exp(-\beta\cos\theta_i)$, with $\bar{C} = 1/\sum_{i,j=1}^{p,q}\exp(-\beta\cos\theta_i)$, the remaining equation is

$$r = \sum_{i,j=1}^{p,q} N_{\theta_i\varphi_j} l\cos\theta_i = N\bar{C}\sum_{i,j=1}^{p,q}\exp(-\beta\cos\theta_i)\, l\cos\theta_i \tag{17}$$

This equation can be written

$$\frac{r}{Nl} = -\frac{d}{d\beta}\left[\ln\sum_{i,j=1}^{p,q}\exp(-\beta\cos\theta_i)\right] \tag{18}$$

as it is immediate to check performing the derivative. Assuming N large, we can take a continuous distribution in the solid angle (to account for equal slots)

$$\sum_{i,j=1}^{p,q}\exp(-\beta\cos\theta_i) \Rightarrow \int_0^{2\pi}\int_0^{\pi}\exp(-\beta\cos\theta)\sin\theta d\theta d\varphi = 4\pi\frac{\sinh\beta}{\beta} \tag{19}$$

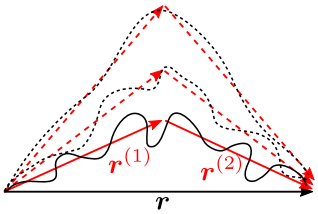

Figure 2: Considering a single chain as two different linked chains. Relevance of the determined end-to-end vector $\boldsymbol{r}$. Note that each $\boldsymbol{r}$ has the mean orientation of the links of the respective chain fractions.

and using Eq. (18)

$$\frac{r}{Nl} = -\frac{d}{d\beta}\ln\left(4\pi\frac{\sinh\beta}{\beta}\right) = \frac{1}{\beta} - \coth\beta = -\mathcal{L}(\beta) \tag{20}$$

where $\mathcal{L}(\bullet)$ is the well-known Langevin function, so the tension f in the chain $f = -TdS/dr = -Tf_T$ takes the well-known expression

$$\beta = -\mathcal{L}^{-1}\left(\frac{r}{Nl}\right) \Rightarrow f := -f_T T = -\frac{\beta k_B}{l}T = \frac{k_B T}{l}\mathcal{L}^{-1}\left(\frac{r}{Nl}\right) \tag{21}$$

A more accurate description follows the Rayleigh distribution; see Kiêm and Itskov (2016) and Sec. 6.5 of Treloar (1975). From a reference configuration with $r = {}^0r$, the tension is obtained with $r = \lambda_{ch}\,{}^0r$, where λ_{ch} is the stretch in the chain respect to the reference configuration. As it is well known, in the Gaussian statistical theory (valid for small fractional extensions typical in unloaded configurations), the unloaded mean chain length is ${}^0r = \sqrt{N}l$; see e.g. Eq. (3.11) in Treloar (1975).

Consider again the partition of the chain in aligned pieces (statistically equivalent segments, meaning equal distribution of links), each with a respective constraint $r^{(k)}$ such that $r = \sum r^{(k)}$ and proportional lengths $Nl = \sum N^{(k)}l$. Following the same steps, we get that each chain partition has a tension $f^{(k)} = (k_B T/l)\,\mathcal{L}^{-1}(\lambda_{ch}^{(k)}/\sqrt{N^{(k)}})$. The total chain length itself Nl (or $N^{(k)}l$) does not play a relevant role: the link length l only affects the leading constant just as k_B, T, but $N^{(k)}$ sets the unstretched location in the inverse Langevin function through $1/\sqrt{N^{(k)}}$ (accounting for the relative number of available configurations, or to tell how far λ_{ch} is from zero entropy). Densely cross-linked or entangled polymers will have a smaller equivalent N (for the representative chain) than loose ones, meaning less possible random configurations for the chain and the whole network. Of course the orientation for each force is along the respective mean chain orientation, that of $\boldsymbol{r}^{(k)}$. Interestingly, if we consider the middle point moving in a direction perpendicular to $\boldsymbol{r}$, there would be no increase in the whole chain r (see Fig.2), but each of the parts would increase their tension. This paradox, is typically solved requiring that chain ends can only be joints of several chains in the network, so internal links in chains can move freely (and very loosely because $\sqrt{N} << N$) in a non-affine manner, but chain joints are forced to move in an affine manner, "tied" to the continuum. This results in a complete different treatment for chains themselves respect to the network as an entity: free fluctuating internal links in a fixed, nonfluctuating network configuration. However, this paradox may also be resolved, as seen below, when the tensions from all the chains are integrated in space allowing the network to fluctuate and considering a chain length mainly as a representation of the possible configurations of the average chain (or chain parts) in the network oriented in such direction. Moreover, the number of links N would be just related to the number of available configurations of the representative single chain, covering the additional possible configurations of the network as a whole, or the decrease of them due to interaction with forest chains.

2.5. The additional configurational entropy of the network

The steps from the previous section are well known, and result in a tension in the chain from the non-isotropic orientation of the chain links produced by the kinematic constraint in the chain r. In Fig. 3a

we show a sketch of a chain network around a given point. Obviously the arrangement is random in the unloading configuration so it is assumed to be isotropic, meaning that there is no preferred orientation in the chains (or more specifically no preferred orientation in the end-to-end or joint-to-joint vector $\boldsymbol{r}$), so they are equally distributed in the solid angle $d\Omega$; see Fig. 3b. Note that there is no need to explicitly take into account chains attaching other chains, because all of them are already considered in the isotropic configuration (e.g. red chain in Fig. 3b).

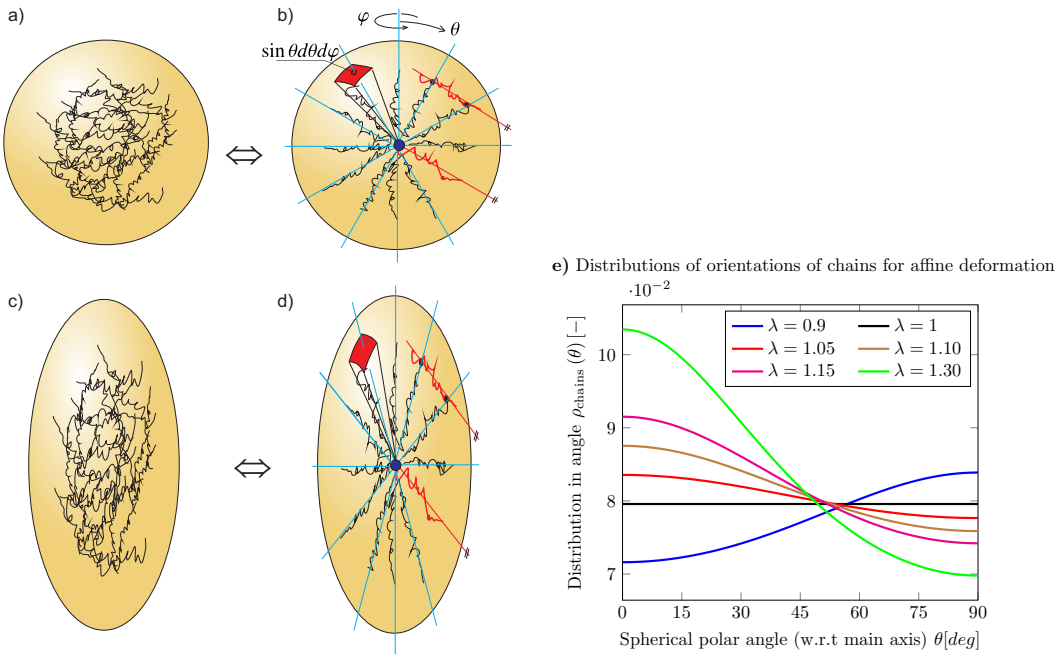

Figure 3: a) Network of chains around a point in the continuum. b) Equivalent isotropic distribution of chains with one end in the continuum point and solid angle $d\Omega = \sin\theta d\theta d\varphi$. c) Deformed continuum around a continuum point, and deformation of the network assuming affine deformations. d) Deformation of the chains and their new angular distribution assuming affine deformations in the network. e) Distribution density of the chains $\rho_{\text{chains}}(\theta)$ for affine deformations, according to the orientation in the space. Note that for $\lambda = 1$ the uniform distribution is recovered. The affine deformation assumption changes the spatial distribution of the chains according to the affine deformation constraint.

During the deformation in a solid, the assumption of spatially isotropic distribution of chains may be considered not valid any more. Affine network deformations assume so, where at least some chain ends of the network are "tied" to the "solid" (which is assumed to be the network itself) instead of maintaining the average isotropic distribution; see Figs. 3c and 3d. This means that there is a constraint in the spatial orientation of the chains in the network given by the macroscopic stretches. As we did with r for constraining the links orientation in the single chain, we introduce the macromechanical kinetic variable describing a chains orientation constraint, say λ. For simplicity in the discussion, we will assume only one degree of freedom, one constraint λ typical from a tensile test along z (in our assumption of an isotropic distribution, this force vanishes). This distribution changes the orientation of the chains following the pattern of the affine deformations performed along z, i.e. a chain of coordinates (now angles refer to the macroscopic tensile axis z)

$$\boldsymbol{r}_0 = r_0\hat{\boldsymbol{r}}_0 = r_0 \begin{bmatrix} \cos\varphi\sin\theta \\ \sin\varphi\sin\theta \\ \cos\theta \end{bmatrix} \tag{22}$$

will change as $\boldsymbol{r} = \boldsymbol{U}_{conf}\boldsymbol{r}_0$, and the differential of surface $d\boldsymbol{s}_0 = ds_0\hat{\boldsymbol{r}}_0 = d\Omega\hat{\boldsymbol{r}}_0$, according to Nanson's formula, as $\boldsymbol{U}_{conf}^{-1}d\boldsymbol{s}_0$ where $\boldsymbol{U}_{conf} = diag(1/\sqrt{\lambda}, 1/\sqrt{\lambda}, \lambda)$. Under the affinity assumption $\boldsymbol{U} = \boldsymbol{U}_{conf}$. We

normalize the density distributions in both the undeformed Ω and the deformed Θ configurations as

$$1 = \int_{\Omega} \rho_{\Omega}(\theta,\varphi)\, d\Omega = \int_{\Theta} \rho_{\Theta}(\theta,\varphi)\, d\Theta \tag{23}$$

If we transform slot-to-slot following the affine relation, since $\rho_{\Omega}(\theta,\varphi) = 1/\Omega$

$$\rho_{\Theta}(\theta,\varphi) = \rho_{\Omega}(\theta,\varphi)\frac{d\Omega}{d\Theta} = \frac{1}{\Omega}\frac{d\Omega}{d\Theta} \tag{24}$$

which means that an increase of surface results in a decrease of chain density towards that orientation (they become more far apart). In general, the surface transformation, as a result of Nanson's formula, is

$$\frac{d\Theta}{d\Omega} = \frac{1}{2}\sqrt{\begin{array}{c}\frac{2}{\lambda_3^2}+\frac{1}{\lambda_2^2}+\frac{1}{\lambda_1^2}+\left(\frac{2}{\lambda_3^2}-\frac{1}{\lambda_2^2}-\frac{1}{\lambda_1^2}\right)\cos 2\theta-\left(\frac{1}{\lambda_1^2}-\frac{1}{\lambda_2^2}\right)\cos 2\varphi+... \\ ...+\left(\frac{1}{2\lambda_1^2}-\frac{1}{2\lambda_2^2}\right)\cos(2\theta-2\varphi)+\left(\frac{1}{2\lambda_1^2}-\frac{1}{2\lambda_2^2}\right)\cos(2\theta+2\varphi)\end{array}} \tag{25}$$

For a prolate ellipsoid, typical of a tensile test under consideration, with $\lambda_1 = \lambda_2 < \lambda_3$

$$\frac{d\Theta}{d\Omega} = \frac{1}{\sqrt{2}}\sqrt{\frac{1}{\lambda_3^2}+\frac{1}{\lambda_1^2}+\left(\frac{1}{\lambda_3^2}-\frac{1}{\lambda_1^2}\right)\cos 2\theta} \tag{26}$$

so taking $\lambda_3 = \lambda = 1/\lambda_1^2 = 1/\lambda_2^2$

$$\rho_{\text{chains}}(\lambda,\theta) \equiv \rho_{\Theta}(\lambda,\theta) = \frac{\sqrt{2}\lambda}{4\pi\sqrt{(\lambda^3+1)+(1-\lambda^3)\cos 2\theta}} \tag{27}$$

This distribution is plotted in Fig. 3e for different values of λ. Note that the affinity assumption produces a strongly anisotropic orientational distribution. The entropy due to the reorientation of chains is

$$S_{conf} = -C_c \int_0^{2\pi}\int_0^{\pi} \rho_{chains}(\lambda,\theta)\ln\rho_{chains}(\lambda,\theta)\sin\theta d\theta d\varphi \tag{28}$$

For having an intuitive view, we define an equivalent configurational stress tensor as

$$\boldsymbol{P}_{conf} = -T\frac{dS_{conf}}{d\boldsymbol{U}_{conf}} = -T\sum_{i=1}^{3}\frac{dS_{conf}}{d\lambda}\left(\frac{d\lambda_i}{d\lambda}\right)^{-1}\hat{\boldsymbol{n}}_i\otimes\hat{\boldsymbol{n}}_i \tag{29}$$

with $(d\lambda_1/d\lambda)^{-1} = (d\lambda_2/d\lambda)^{-1} = -2\lambda^{\frac{3}{2}}$ and $(d\lambda_3/d\lambda)^{-1} = 1$ and

$$\begin{aligned}\frac{dS_{conf}}{d\lambda} &= -C_c\int_0^{2\pi}\int_0^{\pi}\frac{d}{d\lambda}\left[\rho_{chains}(\lambda,\theta)\ln\rho_{chains}(\lambda,\theta)\right]\sin\theta d\theta d\varphi \\ &= C_c\int_0^{2\pi}\int_0^{\pi}P_{chc\theta}(\lambda,\theta)\sin\theta d\theta d\varphi\end{aligned} \tag{30}$$

with

$$P_{chc\theta}(\lambda,\theta) = -\frac{\sqrt{2}}{8\pi}\frac{3(1+\cos 2\theta)-\alpha^2}{\alpha^3}\left(1+\ln\frac{\lambda}{2\sqrt{2}\pi\alpha}\right) \tag{31}$$

where $\alpha = \sqrt{\cos 2\theta+\lambda^3-\lambda^3\cos 2\theta+1}$. Note that $-TdS_{conf}/d\lambda$ is the generalized force due to the orientational constraint. To arrive to a compact expression (the accuracy is not relevant for the discussion), we take the Taylor series in $(\lambda-1)$. The constant term in the integral vanishes, and the other terms are

$$\frac{dS_{conf}}{d\lambda} = 0 - \frac{C_c}{5}(\lambda-1)(2\ln 4\pi-1) - \frac{C_c}{70}(\lambda-1)^2(44\ln 4\pi-18) + O\left((\lambda-1)^3\right) \tag{32}$$

Then, retaining the first term, dominant for small stretches, we can convert $-TdS_{conf}/d\lambda$ to the orientational configuration stress tensor (up to the pressure-like Lagrangian whose related constraint should be enforced in the complete stress tensor), which is

$$\boldsymbol{P}_{conf} = -T\frac{dS_{conf}}{d\boldsymbol{U}_{conf}} = T\hat{C}\left(\lambda-1\right)\begin{bmatrix} -2\lambda^{\frac{3}{2}} & & \\ & -2\lambda^{\frac{3}{2}} & \\ & & 1 \end{bmatrix} + O\left(\left(\lambda-1\right)^2\right) \tag{33}$$

where $\hat{C}$ is a new constant.

Equation (33) simply shows the observation that the constraint associated to an affine redistribution of the orientation of the chains produces a stress tensor tied to the *additional configurational entropy of the network*. This is a result that should be expected when comparing with the force obtained from the constraint r associated to the *configurational entropy of the single chain*. Remarkably, affine models do not consider (at least explicitly) the generalized force associated to the entropic term $-TdS_{conf}$ related to the configurational entropy of the network, despite deviating from the isotropic distribution and constraining the chains distribution to that of the continuum. If this network configurational stress is not considered, then the (unconstrained) isotropic distribution in the orientation of the chains should be preserved. Note that the tensor, if considered per-chain, means that the equivalent force in a chain for an affine model in which the configurational entropy is considered, is in general not aligned with $\boldsymbol{r}$. Conceptually, this would be the force tied to the biased statistical rotations of the chains.

3. Macro-micro connection: the chain stretch

The previous section describes the tension in the chains according to the fractional extension $r/\left(Nl\right)$, where r is the end-to-end chain distance, the modulus of $\boldsymbol{r}$. In this section we perform the connection of the stretch and tension in the chains to the deformation and stress in the continuum.

3.1. Homogenization of chain tensions

Consider $\boldsymbol{r}\left(t\right) = \lambda_{ch}\left(t\right)\hat{\boldsymbol{r}}\left(t\right)$ with modulus $\lambda_{ch}\left(t\right)$ and with direction $\hat{\boldsymbol{r}}\left(t\right) = \boldsymbol{r}\left(t\right)/\lambda_{ch}\left(t\right)$. The derivative is

$$\dot{\boldsymbol{r}} = \dot{\lambda}_{ch}\left(t\right)\hat{\boldsymbol{r}}\left(t\right) + \lambda_{ch}\left(t\right)\frac{d\hat{\boldsymbol{r}}\left(t\right)}{dt} \tag{34}$$

where we may consider the Gaussian solution $\left|\boldsymbol{r}\left(0\right)\right| = \sqrt{N}l$, so $\lambda_{ch}\left(t\right) = \left|\boldsymbol{r}\left(t\right)\right|/\sqrt{N}l$, but in practice it is irrelevant to this discussion, so for generality we may just think of relative values, e.g. $r(0) = \lambda_{ch}(0) = 1$. Defining $\boldsymbol{t}_{ch}$ as the tension vector in the chain, the power spent in changing the entropy of a single chain is

$$\mathcal{P}_{ch} = \boldsymbol{t}_{ch}\cdot\dot{\boldsymbol{r}} = \dot{\lambda}_{ch}\boldsymbol{t}_{ch}\cdot\hat{\boldsymbol{r}} + \lambda_{ch}\boldsymbol{t}_{ch}\cdot\frac{d\hat{\boldsymbol{r}}}{dt} \tag{35}$$

Define the averaging (homogenization) operator as

$$\bar{\mathcal{A}} \equiv \langle\mathcal{A}\rangle = \int_{\Omega}\mathcal{A}\frac{d\Omega}{\Omega} \tag{36}$$

where $\mathcal{A}$ is any entity (scalar, vectorial or tensorial) and $d\Omega/\Omega$ is the weight of each contribution, assumed proportional to its share of solid area. Then, in order to connect the micro structure with the continuum, the following identity is proposed

$$\mathcal{P}_{ext} = \tfrac{1}{2}\boldsymbol{S}:\dot{\boldsymbol{C}} = \bar{\mathcal{P}} \equiv \langle\mathcal{P}_{ch}\rangle = \int_{\Omega}\mathcal{P}_{ch}\frac{d\Omega}{\Omega} = \int_{\Omega}\dot{\lambda}_{ch}\boldsymbol{t}_{ch}\cdot\hat{\boldsymbol{r}}\frac{d\Omega}{\Omega} + \int_{\Omega}\lambda_{ch}\boldsymbol{t}_{ch}\cdot\frac{d\hat{\boldsymbol{r}}}{dt}\frac{d\Omega}{\Omega} \tag{37}$$

From the previous expression, two addends can be identified. The first one is the power spent in the chains length change, λ_{ch}. The second term represents the work spent in the rotations of the chains $d\hat{\boldsymbol{r}}/dt$.

No assumption about the origin of $\boldsymbol{t}_{ch}$ has been made so far. If the existence of a potential function for every chain is assumed, i.e., there exists $\psi_{ch}(\boldsymbol{r})$ (e.g. such that $\dot{\psi}_{ch} = -T\dot{S}_{ch}$ as typically assumed), by frame invariance we must also assume that the energy stored in a chain is independent of the observer, $\psi_{ch}(\boldsymbol{r}) = \psi_{ch}(\boldsymbol{Q}\boldsymbol{r})\ \forall \boldsymbol{Q} \in \mathrm{Orth}^{+}$. The vector modulus is the only invariant with respect to the transformations in Orth^{+}, therefore, to satisfy the previous condition, $\psi_{ch}(\boldsymbol{r}) = \psi_{ch}(|\boldsymbol{r}|) = \psi_{ch}(\lambda_{ch})$. If $\boldsymbol{t}_{ch}$ derives from such energy, it is the work conjugate of $\boldsymbol{r}$, so $\boldsymbol{t}_{ch} := d\psi_{ch}/d\boldsymbol{r}$:

$$\boldsymbol{t}_{ch} := \frac{d\psi_{ch}(|\boldsymbol{r}|)}{d\boldsymbol{r}} = \frac{d\psi_{ch}(|\boldsymbol{r}|)}{d|\boldsymbol{r}|}\frac{d|\boldsymbol{r}|}{d\boldsymbol{r}} = \frac{d\psi_{ch}(\lambda_{ch})}{d\lambda_{ch}}\frac{d|\boldsymbol{r}|}{d\boldsymbol{r}} = \frac{d\psi_{ch}}{d\lambda_{ch}}\hat{\boldsymbol{r}} \tag{38}$$

where we used $d\left(\sqrt{\boldsymbol{r}\cdot\boldsymbol{r}}\right)/d\boldsymbol{r} = \hat{\boldsymbol{r}}$ and $d\hat{\boldsymbol{r}}/d\boldsymbol{r} = \boldsymbol{I} - \hat{\boldsymbol{r}}\otimes\hat{\boldsymbol{r}} = \boldsymbol{P}_{\hat{\boldsymbol{r}}}$ is the projector on the plane perpendicular to $\hat{\boldsymbol{r}}$. Therefore, Eqs. (37) and (38), along the condition $\hat{\boldsymbol{r}} \perp d\hat{\boldsymbol{r}}/dt$, give

$$\mathcal{P}_{ext} = \bar{\mathcal{P}} = \langle \mathcal{P}_{ch} \rangle = \int_{\Omega} \mathcal{P}_{ch}\frac{d\Omega}{\Omega} = \int_{\Omega} \dot{\lambda}_{ch}\frac{d\psi_{ch}}{d\lambda_{ch}}\frac{d\Omega}{\Omega} = \frac{1}{\Omega}\int_{\Omega}\dot{\psi}_{ch}d\Omega \tag{39}$$

Noteworthy, the chains rotation term in the power equation is zero because the individual rotation of every single chain considered in the model cannot produce a variation in the entropy of that chain if only the chain entropy change is considered (i.e. the network entropy configuration due to chains orientation is neglected).

The micromechanical variable λ_{ch} remains to be linked to the continuum (micro-macro connection) and it can be done in multiple ways. We consider two approaches. One way to determine the continuum strain energy of the solid from the microstructural quantities could be an averaging scheme. Considering only the configurational entropy of the chains themselves to build the overall one, we have the potential

$$\Psi(\boldsymbol{V}) = \Psi(\boldsymbol{U}) = \langle \psi_{ch} \rangle = \frac{1}{\Omega}\int_{\Omega}\psi_{ch}(\boldsymbol{r})\,d\Omega = \frac{1}{\Omega}\int_{\Omega}\psi_{ch}(\hat{\boldsymbol{r}},\boldsymbol{U})\,d\Omega \tag{40}$$

where Ω is the unit sphere surface, $\psi_{ch}(\boldsymbol{r})$ is the energy density of the chains laid along direction $\hat{\boldsymbol{r}}$ and $d\Omega$ is the surface differential of unit sphere surface (isotropic distribution), with direction (perpendicular to) $\hat{\boldsymbol{r}}$, so $d\Omega/\Omega$ is the corresponding weight assigned to the chains in direction $\hat{\boldsymbol{r}}$. The tensor $\boldsymbol{U}$ is the stretch of the continuum, and by $\psi_{ch}(\hat{\boldsymbol{r}},\boldsymbol{U})$ we are stating that in a way determined below, the chain energy is related to the continuum stretches given by the stretch tensor from the polar decomposition. Note that we use frequently the same symbols for different functions with same physical meaning. We do so to avoid proliferation of symbols and decorations; we leave the arguments explicit if confusion is possible.

If we assign to the chain a constant surface $d\Omega$ (representing the weight or reference density of chains with the given orientation $\hat{\boldsymbol{r}}$), then the force is $d\boldsymbol{f}_{ch} = \boldsymbol{t}_{ch}(\boldsymbol{r})\,d\Omega$. Then, we can define a stress tensor

$$\boldsymbol{P}_{ch} = \frac{d\psi_{ch}}{d\lambda_{ch}}\hat{\boldsymbol{r}}\otimes\hat{\boldsymbol{r}} =: P_{ch}\hat{\boldsymbol{r}}\otimes\hat{\boldsymbol{r}} \ \text{ such that } d\boldsymbol{f}_{ch} = \boldsymbol{P}_{ch}\cdot\hat{\boldsymbol{r}}\ d\Omega \tag{41}$$

The force for the chains at orientation $\hat{\boldsymbol{r}}$ is

$$d\boldsymbol{f}_{ch} = \boldsymbol{P}_{ch}\cdot\ \hat{\boldsymbol{r}}\ d\Omega = \boldsymbol{t}_{ch}d\Omega = \frac{d\psi_{ch}}{d\lambda_{ch}}\hat{\boldsymbol{r}}d\Omega \tag{42}$$

and $d\boldsymbol{f}_{ch}$ is to be integrated. The averaged power (power density) is —cf. Eq. (39)

$$\begin{aligned}\bar{\mathcal{P}} = \frac{1}{\Omega}\int_{\Omega} d\boldsymbol{f}_{ch}\cdot\dot{\lambda}_{ch}\hat{\boldsymbol{r}}d\Omega &= \frac{1}{\Omega}\int_{\Omega}\dot{\lambda}_{ch}\hat{\boldsymbol{r}}\cdot\boldsymbol{P}_{ch}\cdot\hat{\boldsymbol{r}}d\Omega \\ &= \frac{1}{\Omega}\int_{\Omega}\frac{d\psi_{ch}}{d\lambda_{ch}}\dot{\lambda}_{ch}d\Omega = \frac{1}{\Omega}\int_{\Omega}\dot{\psi}_{ch}d\Omega\end{aligned} \tag{43}$$

Thus, let us define the average stress tensor —see Eq. (40)

$$\bar{\boldsymbol{P}}_{ch} = \langle \boldsymbol{P}_{ch} \rangle = \int_{\Omega}\boldsymbol{P}_{ch}\frac{d\Omega}{\Omega} = \int_{\Omega}\frac{d\psi_{ch}}{d\lambda_{ch}}\hat{\boldsymbol{r}}\otimes\hat{\boldsymbol{r}}\frac{d\Omega}{\Omega} =: \frac{d\Psi}{d\boldsymbol{U}} \tag{44}$$

During a tensile, biaxial or pure shear test in an incompressible continuum, (to eliminate macroscopic rotations in the reasoning such that $\boldsymbol{R}=\boldsymbol{I}$ and $\boldsymbol{F}=\boldsymbol{U}$), the Piola stress is

$$\boldsymbol{P}=\frac{d\Psi}{d\boldsymbol{F}}+p\boldsymbol{F}^{-1}=\frac{d\Psi}{d\boldsymbol{U}}+p\boldsymbol{U}^{-1}\Rightarrow\ P_i=\frac{\partial\Psi}{\partial\lambda_i}+\frac{1}{\lambda_i}p \tag{45}$$

where p is the pressure-like Lagrange multiplier for the incompressibility condition. Then

$$\begin{aligned}P_i=\frac{1}{\lambda_i}p+\frac{\partial\Psi}{\partial\lambda_i}&=\frac{1}{\lambda_i}p+\hat{\boldsymbol{n}}_i\cdot\bar{\boldsymbol{P}}_{ch}\cdot\hat{\boldsymbol{n}}_i\\&=\frac{1}{\lambda_i}p+\int_\Omega\frac{d\psi_{ch}}{d\lambda_{ch}}\left(\hat{\boldsymbol{r}}\cdot\hat{\boldsymbol{n}}_i\right)^2\frac{d\Omega}{\Omega}\end{aligned} \tag{46}$$

where $\hat{\boldsymbol{r}}$ is the orientation of chains, to which a constant isotropic weight of $d\Omega/\Omega$ has been assigned.

3.2. The isotropic micro-macro connection for the chain stretch

Taking the following definition for the stretch

$$\lambda_{ch}\left(\hat{\boldsymbol{r}}\right)=\boldsymbol{U}:\hat{\boldsymbol{r}}\otimes\hat{\boldsymbol{r}}=\left(\sum_{i=1}^{3}\lambda_i\hat{\boldsymbol{n}}_i\otimes\hat{\boldsymbol{n}}_i\right):\left(\hat{\boldsymbol{r}}\otimes\hat{\boldsymbol{r}}\right)=\sum_{i=1}^{3}\lambda_i\left(\hat{\boldsymbol{r}}\cdot\hat{\boldsymbol{n}}_i\right)^2 \tag{47}$$

it is immediate to check that we recover Eq. (46) by direct use of the chain rule

$$P_i\equiv\frac{1}{\lambda_i}p+\frac{d\Psi}{d\lambda_i}=\frac{1}{\lambda_i}p+\frac{1}{\Omega}\int_\Omega\frac{d\psi_{ch}}{d\lambda_{ch}}\frac{d\lambda_{ch}}{d\lambda_i}d\Omega=\frac{1}{\lambda_i}p+\frac{1}{\Omega}\int_\Omega\frac{d\psi_{ch}}{d\lambda_{ch}}\left(\hat{\boldsymbol{r}}\cdot\hat{\boldsymbol{n}}_i\right)^2d\Omega \tag{46}$$

which is consistent also with the definition in Eq. (40). In essence, $\hat{\boldsymbol{r}}$ plays the role of a direction in the sphere (not that of a particular chain) and λ_{ch} of the stretch associated to that direction. No change in weights is assumed: physically it may be interpreted as that the isotropic distribution is maintained, because no force is considered to rotate the chains and entropy is only considered regarding the constraint r in direction $\hat{\boldsymbol{r}}$ for each chain.

Note that once the relation $P_i\left(\lambda_1,\lambda_2\right)$ has been obtained, it is of course valid not only for the mentioned tests, but for any boundary or deformation condition found in any stress integration point in a finite element program. Obviously, the stress power density is also equivalent. Since in these tests, principal directions are rotationless and there is no volumetric power (by incompressibility), we verify

$$\begin{aligned}\mathcal{P}\equiv\dot{\Psi}=\sum_{i=1}^{3}P_i\dot{\lambda}_i&=\sum_{i=1}^{3}\frac{d\Psi}{d\lambda_i}\dot{\lambda}_i+\sum_{i=1}^{3}p\frac{\dot{\lambda}_i}{\lambda_i}\\&=\sum_{i=1}^{3}\left(\frac{1}{\Omega}\int_\Omega\frac{d\psi_{ch}}{d\lambda_{ch}}\frac{d\lambda_{ch}}{d\lambda_i}d\Omega\right)\ \dot{\lambda}_i+p\sum_{i=1}^{3}\frac{d}{dt}\left(\ln\lambda_i\right)\end{aligned} \tag{48}$$

$$\begin{aligned}&=\frac{1}{\Omega}\int_\Omega\frac{d\psi_{ch}}{d\lambda_{ch}}\left(\sum_{i=1}^{3}\frac{d\lambda_{ch}}{d\lambda_i}\dot{\lambda}_i\right)\ d\Omega+0\\&=\frac{1}{\Omega}\int_\Omega\frac{d\psi_{ch}}{d\lambda_{ch}}\dot{\lambda}_{ch}\ d\Omega\quad=\frac{1}{\Omega}\int_\Omega\dot{\psi}_{ch}\ d\Omega=\bar{\mathcal{P}}\ \ \text{(see Eqs. (39) and (43))}\end{aligned} \tag{49}$$

3.3. The affine micro-macro connection for the chain stretch

The usually employed alternative is to assume affinity in the right Cauchy-Green deformation tensor obtained from the following micro-macro relation. Because now $\hat{\boldsymbol{r}}$ is attached to the continuum and a specific chain, in this case it is important to distinguish the original direction ${}^0\hat{\boldsymbol{r}}$ corresponding to the continuum-undeformed configuration, and the current deformed one $\hat{\boldsymbol{r}}$

$$\lambda_{ch}\left(\hat{\boldsymbol{r}}\right)\ \hat{\boldsymbol{r}}=\boldsymbol{R}\boldsymbol{U}\cdot\ {}^0\hat{\boldsymbol{r}} \tag{50}$$

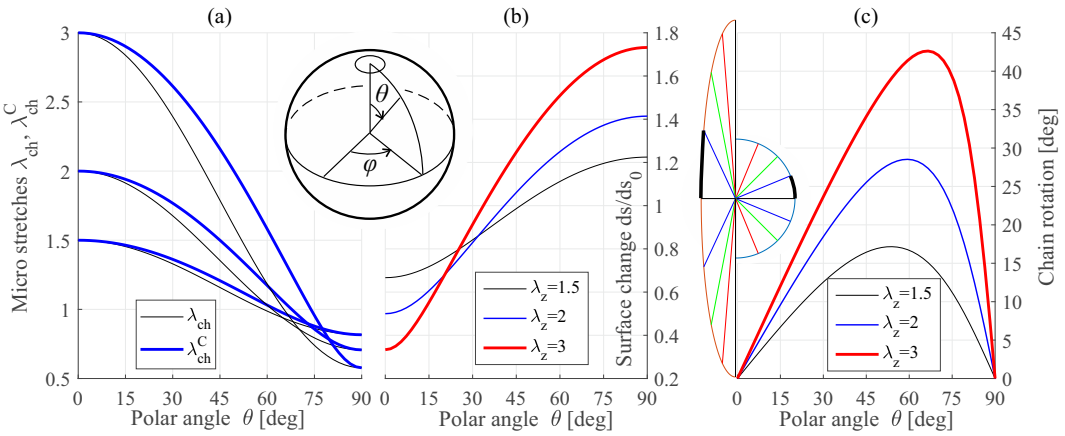

Figure 4: a) Difference between $\lambda_{ch} = \hat{\boldsymbol{r}} \cdot \boldsymbol{U} \cdot \hat{\boldsymbol{r}}$ and $\lambda^C_{ch} = \sqrt{\hat{\boldsymbol{r}} \cdot \boldsymbol{C} \cdot \hat{\boldsymbol{r}}}$ for different uniaxial stretches $\lambda_z = 1.5$, $\lambda_z = 2$, $\lambda_z = 3$. b) Change of surface due to surface-affine deformations. c) Rotation of chains if they follow affine deformations.

so, multiplying by the transpose to cancel the continuum rotations, we identify the affine squared stretches from the Cauchy-Green deformation tensor in the chain direction

$$\Lambda_{ch} = {}^0\hat{\boldsymbol{r}} \cdot \boldsymbol{C} \cdot {}^0\hat{\boldsymbol{r}} := \left(\lambda^C_{ch}\right)^2 = \sum_{i=1}^{3} \Lambda_i \left(\hat{\boldsymbol{n}}_i \cdot {}^0\hat{\boldsymbol{r}}\right)^2 \tag{51}$$

where Λ_i are the eigenvalues of $\boldsymbol{C}$. These stretches assume deformations affine with the continuum deformation gradient. In general, for chains not aligned with the principal directions —see Fig. 4a

$$\lambda^C_{ch}\left({}^0\hat{\boldsymbol{r}}\right) = \sqrt{{}^0\hat{\boldsymbol{r}} \cdot \boldsymbol{C} \cdot {}^0\hat{\boldsymbol{r}}} \neq {}^0\hat{\boldsymbol{r}} \cdot \boldsymbol{U} \cdot {}^0\hat{\boldsymbol{r}} = \lambda_{ch}\left({}^0\hat{\boldsymbol{r}}\right) \tag{52}$$

Note that even though $\boldsymbol{R} = \boldsymbol{I}$ we have that necessarily a superposed rotation $\boldsymbol{R}_{ch} \neq \boldsymbol{I}$ for chains not aligned in principal directions, because $\boldsymbol{U} \cdot {}^0\hat{\boldsymbol{r}}$ does not have the direction of ${}^0\hat{\boldsymbol{r}}$; Fig. 4c shows that this rotation is important. Indeed, this is a basic difference between both approaches: whether the rotations of the chains follow the continuum line rotations or if these rotations (which do not produce work according to this framework) are such that the distribution remains isotropic (i.e. chains fluctuate freely). Of course, intermediate cases are also possible, depending on the relative importance of the system network entropy respect to the entropy of the chains.

Then, if we assume that Λ_{ch} (or λ^C_{ch}) is the state variable for the deformation in the chains, then we can define —cf. Eq. (41)

$$\boldsymbol{S}_{ch} := 2\frac{d\psi_{ch}}{d\Lambda_{ch}}\, {}^0\hat{\boldsymbol{r}} \otimes {}^0\hat{\boldsymbol{r}} \tag{53}$$

and further define an averaged second Piola-Kirchhoff (PK) stress by integration in the unit sphere as —cf. Eq. (44)

$$\begin{aligned}\bar{\boldsymbol{S}}_{ch} = \langle \boldsymbol{S}_{ch} \rangle &= \int_\Omega \boldsymbol{S}_{ch} \frac{d\Omega}{\Omega} = \frac{1}{\Omega}\int_\Omega 2\frac{d\psi_{ch}}{d\Lambda_{ch}}\, {}^0\hat{\boldsymbol{r}} \otimes {}^0\hat{\boldsymbol{r}} d\Omega \\ &= \frac{1}{\Omega}\int_\Omega 2\frac{d\psi_{ch}}{d\Lambda_{ch}}\frac{d\Lambda_{ch}}{d\boldsymbol{C}} d\Omega = \frac{1}{\Omega}\int_\Omega \frac{1}{\lambda^C_{ch}}\frac{d\psi_{ch}}{d\lambda^C_{ch}}\, {}^0\hat{\boldsymbol{r}} \otimes {}^0\hat{\boldsymbol{r}} d\Omega\end{aligned} \tag{54}$$

This is the typical chain rule and approach followed in the affine approach; see e.g. Eq. (128) of Steinmann et al. (2012). It is also the typical additive scheme in terms of 2nd Piola-Kirchhoff stresses employed in soft tissues as chained derivatives of energy terms taken respect to Rivlin-Spencer invariants of $\boldsymbol{C}$; see e.g. Holzapfel (2000), Eq. (12) in Chagnon et al. (2015), Eq. (5.9) in Volokh (2016) and therein referenced models. Note that this is equivalent to assigning a surface weight $d\Omega/\lambda^C_{ch}$ to the chain, an expression which

would also follow applying Nanson's formula to the chain stretch considering the deformation gradient of the chain. Then, we assume that the principal values of the continuum 2nd PK stresses are given by —cf. its push-forward $\sigma_i = \lambda_i^2 S_i$ in Eq. (4) of Wu and van der Giessen (1992)

$$\begin{aligned} S_i = \frac{1}{\lambda_i^2}p + 2\frac{d\Psi}{d\Lambda_i} &= \frac{1}{\lambda_i^2}p + \bar{\boldsymbol{S}}_{ch} : \hat{\boldsymbol{n}}_i \otimes \hat{\boldsymbol{n}}_i \\ &= \frac{1}{\lambda_i^2}p + \left(\frac{1}{\Omega}\int_\Omega 2\frac{d\psi_{ch}}{d\Lambda_{ch}}\ {}^0\hat{\boldsymbol{r}} \otimes\ {}^0\hat{\boldsymbol{r}}\ d\Omega\right) : \hat{\boldsymbol{n}}_i \otimes \hat{\boldsymbol{n}}_i \\ &= \frac{1}{\lambda_i^2}p + \frac{1}{\Omega}\int_\Omega \frac{1}{\lambda_{ch}^C}\frac{d\psi_{ch}}{d\lambda_{ch}^C}\left(\hat{\boldsymbol{n}}_i \cdot\ {}^0\hat{\boldsymbol{r}}\right)^2 d\Omega \end{aligned} \tag{55}$$

It is obvious that the averaging methods of Eq. (46) and Eq. (55) are different, as they are also $\lambda_{ch}\left({}^0\hat{\boldsymbol{r}}\right)$ and $\lambda_{ch}^C\left({}^0\hat{\boldsymbol{r}}\right)$; and λ_{ch} cannot be written as a scalar function of λ_{ch}^C (and vice-versa) because all the principal stretches (or invariants) are involved in the relation.

The stress power in this case is —cf. Eq. (49)

$$\begin{aligned} \mathcal{P} \equiv \dot{\Psi} = \sum_{i=1}^{3}\tfrac{1}{2}S_i\dot{\Lambda}_i = \sum_{i=1}^{3}\frac{d\Psi}{d\Lambda_i}\dot{\Lambda}_i &= \sum_{i=1}^{3}\left(\frac{1}{\Omega}\int_\Omega \frac{d\psi_{ch}}{d\Lambda_{ch}}\frac{d\Lambda_{ch}}{d\Lambda_i}\ d\Omega\right)\ \dot{\Lambda}_i \\ &= \frac{1}{\Omega}\int_\Omega \frac{d\psi_{ch}}{d\Lambda_{ch}}\left(\sum_{i=1}^{3}\frac{d\Lambda_{ch}}{d\Lambda_i}\dot{\Lambda}_i\right)\ d\Omega \\ &= \frac{1}{\Omega}\int_\Omega \frac{d\psi_{ch}}{d\Lambda_{ch}}\dot{\Lambda}_{ch}\ d\Omega = \frac{1}{\Omega}\int_\Omega \dot{\psi}_{ch}\ d\Omega = \bar{\mathcal{P}} \end{aligned} \tag{56}$$

Interestingly, we can push-forward the averaged stress in Eq. (54) to obtain the Piola stress through the continuum mapping, which in the standard tests with $\boldsymbol{R} = \boldsymbol{I}$ is, without the pressure term

$$\begin{aligned} \boldsymbol{F}\bar{\boldsymbol{S}}_{ch} = \boldsymbol{U}\bar{\boldsymbol{S}}_{ch} &= \frac{1}{\Omega}\int_\Omega 2\frac{d\psi_{ch}}{d\Lambda_{ch}}\boldsymbol{U}\frac{d\Lambda_{ch}}{d\boldsymbol{C}}d\Omega \\ &= \frac{1}{\Omega}\int_\Omega \frac{1}{\lambda_{ch}^C}\frac{d\psi_{ch}}{d\lambda_{ch}^C}\sum_{i=1}^{3}\left[\lambda_i\left(\hat{\boldsymbol{n}}_i \cdot\ {}^0\hat{\boldsymbol{r}}\right)\hat{\boldsymbol{n}}_i \otimes\ {}^0\hat{\boldsymbol{r}}\right] d\Omega \end{aligned} \tag{57}$$

If applied to a principal plane, principal direction in the standard homogeneous test

$$\begin{aligned} P_i = \frac{p}{\lambda_i} + \hat{\boldsymbol{n}}_i \cdot \left(\boldsymbol{F}\bar{\boldsymbol{S}}_{ch}\right)\cdot\hat{\boldsymbol{n}}_i &= \frac{p}{\lambda_i} + \frac{1}{\Omega}\int_\Omega \frac{\lambda_i}{\lambda_{ch}^C}\frac{d\psi_{ch}}{d\lambda_{ch}^C}\left(\hat{\boldsymbol{n}}_i \cdot\ {}^0\hat{\boldsymbol{r}}\right)^2 d\Omega \\ &= \frac{p}{\lambda_i} + \frac{\lambda_i}{\Omega}\int_\Omega \frac{d\psi_{ch}}{d\lambda_{ch}^C}\left(\hat{\boldsymbol{n}}_i \cdot\ {}^0\hat{\boldsymbol{r}}\right)^2 \frac{d\Omega}{\lambda_{ch}^C} \end{aligned} \tag{58}$$

which is to be compared to Eq. (46). Note that, (1) the surfaces Ω and $d\Omega$ are now weighted according to their stretches λ_i and λ_{ch}^C, see Fig. 4b; and (2) the chain stretches λ_{ch} and λ_{ch}^C are very different: there is no one-to-one relation between them for a general chain direction, see Fig. 4a. These two differences, respectively, could possibly be behind the needed non-affine micro-macro correction of the *"macro-area-stretch"* (Eqs. (58)-(60) in Miehe et al. (2004)) and the non-affine micro-macro correction of the *"macro-stretch"* (Eqs. (45)-(47) in Miehe et al. (2004)) to accommodate macroscopic experimental results via maximization of the entropy respect to an assumed fluctuation field (Sec. 4.3.2 in Miehe et al. (2004)).

Of course, an intermediate option regarding orientational affinity is possible, although not explored. For example using $\lambda_{ch}^* = (\boldsymbol{U}^p : \hat{\boldsymbol{n}} \otimes \hat{\boldsymbol{n}})^{1/p}$, with $p = 2$ for the affine case and $p = 1$ for the unconstrained case. In general p may be a function of the network characteristics and of the deformation. However, note that solutions of this type are different from the typical non-affine stretches in the literature.

4. The relevance of the choice of the chain stretch in general deformations

4.1. Comparison of two examples of micro-macro connection

In a phenomenological model, $\Psi(\lambda_1,\lambda_2,\lambda_3)$ and $\Psi(\Lambda_1,\Lambda_2,\Lambda_3)$ are mathematically different functions but may be made physically equivalent, because arguments are related in a one-to-one pattern, namely $\Lambda_i = \left(\lambda_i^C\right)^2 = \lambda_i^2$. However, in chain models, different chain stretch variables give physically different models, see Eq. (52) and Fig. 4c

$$\Psi^{(1)}(\boldsymbol{C}) = \frac{1}{\Omega}\int_\Omega \psi_{ch}^{(1)}(\Lambda_{ch})\,d\Omega \neq \frac{1}{\Omega}\int_\Omega \psi_{ch}^{(2)}(\lambda_{ch})\,d\Omega = \Psi^{(2)}(\boldsymbol{U}) \tag{59}$$

Since in principal directions of deformation $\lambda_{ch}^2 = (\lambda_{ch}^C)^2 = \Lambda_{ch}$, and by Fig. 4a differences between both stretches are not very large, one may think that the practical relevance of this observation in the predictions of a model should be small. To investigate this, consider two simple models in which the strain energy is considered only due to the sum of the entropy of the individual chains

$$\psi_{ch}^{(M1)}(\Lambda_{ch}) = \frac{3\mu}{2}(\Lambda_{ch}-1) \quad \text{with} \quad \Lambda_{ch} = \boldsymbol{C}:(\hat{\boldsymbol{r}}\otimes\hat{\boldsymbol{r}}) = (\lambda_{ch}^C)^2 \tag{60}$$

$$\psi_{ch}^{(M2)}(\lambda_{ch}) = \frac{3\mu}{2}\left(\lambda_{ch}^2-1\right) \quad \text{with} \quad \lambda_{ch} = \boldsymbol{U}:(\hat{\boldsymbol{r}}\otimes\hat{\boldsymbol{r}}) \tag{61}$$

from which the macroscopic energies $\alpha = 1,2$ follow by $\Psi^{(\alpha)}(\bullet) = \frac{1}{\Omega}\int_\Omega \psi_{ch}^{(\alpha)}(\bullet)\,d\Omega$, and the derivatives respect to the principal continuum stretches are

$$\frac{\partial\Psi^{(M1)}(\lambda_1,\lambda_2,\lambda_3)}{\partial\lambda_i} = \frac{1}{\Omega}\int_\Omega \frac{d\psi^{(M1)}(\Lambda_{ch})}{d\Lambda_{ch}}\frac{\partial\Lambda_{ch}}{\partial\lambda_i}d\Omega \tag{62}$$

$$\frac{\partial\Psi^{(M2)}(\lambda_1,\lambda_2,\lambda_3)}{\partial\lambda_i} = \frac{1}{\Omega}\int_\Omega \frac{\psi^{(M2)}(\lambda_{ch})}{d\lambda_{ch}}\frac{\partial\lambda_{ch}}{\partial\lambda_i}d\Omega \tag{63}$$

Both models would be identical if $\lambda_{ch} = \lambda_{ch}^C$. The macroscopic predictions may be obtained through a numerical angular integration, see Amores et al. (2020). However, it is well known that

$$\frac{1}{\Omega}\int_\Omega \Lambda_{ch}d\Omega = \frac{1}{3}I_1 \tag{64}$$

where I_1 is the first invariant of $\boldsymbol{C}$. Therefore $\Psi^{(M1)}(\lambda_1,\lambda_2,\lambda_3)$ may also be integrated analytically. The result is the well-known Neo-Hookean model, which is the model obtained from the classical Gaussian network theory, where $\mu = nk_BT$ (n being the chain density)—see Sec. 4.2, Eq. (4.9a) of Treloar (1975)

$$\Psi^{(M1)}(\lambda_1,\lambda_2,\lambda_3) \equiv \Psi^{(\text{N-H})}(\lambda_1,\lambda_2,\lambda_3) = \frac{\mu}{2}(I_1-3) \tag{65}$$

Model M2 would be also a Gaussian model but considering an unconstrained orientational distribution of chains. For the incompressible materials at hand, $P_3 = 0$ will be enforced for all the deformation states considered to eliminate the pressure-like penalization term from the equations, leading to the following set of equations for computing the nominal stresses in principal directions of deformation

$$P_i = \frac{\partial\Psi(\lambda_1,\lambda_2,\lambda_3)}{\partial\lambda_i} - \frac{\lambda_3}{\lambda_i}\frac{\partial\Psi(\lambda_1,\lambda_2,\lambda_3)}{\partial\lambda_3}; \quad i=1,2 \tag{66}$$

To evaluate the aforementioned influence of the independent chain variable used to describe the problem, two states of deformation are computed for the constant $\mu = 1\,\text{MPa}$. For these comparisons we consider two tests defining two families of states of deformation, both with $P_3 = 0$ and complying with the incompressibility constraint

- s1: biaxial test in which $\lambda_2 = 3.1$ and λ_1 varies in the range from 0.2 to 3.1, and $\lambda_3 = 1/(\lambda_1\lambda_2)$
- s2: uniaxial test in which λ_1 will be in the range from 0.8 to 2.2 and $\lambda_2 = \lambda_3 = 1/\sqrt{\lambda_1}$

The biaxial test (s1) is interesting because keeping $\lambda_2 = 3.1$ for all the range of λ_1, the angular distribution of the chains under the affinity assumption is not isotropic in the testing plane $1-2$ (except for the specific point $\lambda_1 = 3.1$). In the uniaxial test (s2), the distribution is isotropic at the beginning of the loading, for $\lambda_1 = 1$. Hence, to emphasize the differences between models, in the sections below we will use the $P_1 - \lambda_1$ curve of the biaxial (s1) test to characterize the materials.

For angular integration in the sphere, we used the 21 points from Bazant and Oh (1986). We plot the two non-vanishing nominal stresses, namely the longitudinal one P_1 (in the axis of main varying stretch) and the transverse one P_2. Using both M1 and M2 models, the nominal stresses P_1 and P_2 obtained for both (s1) and (s2) tests are presented in Fig. 5.

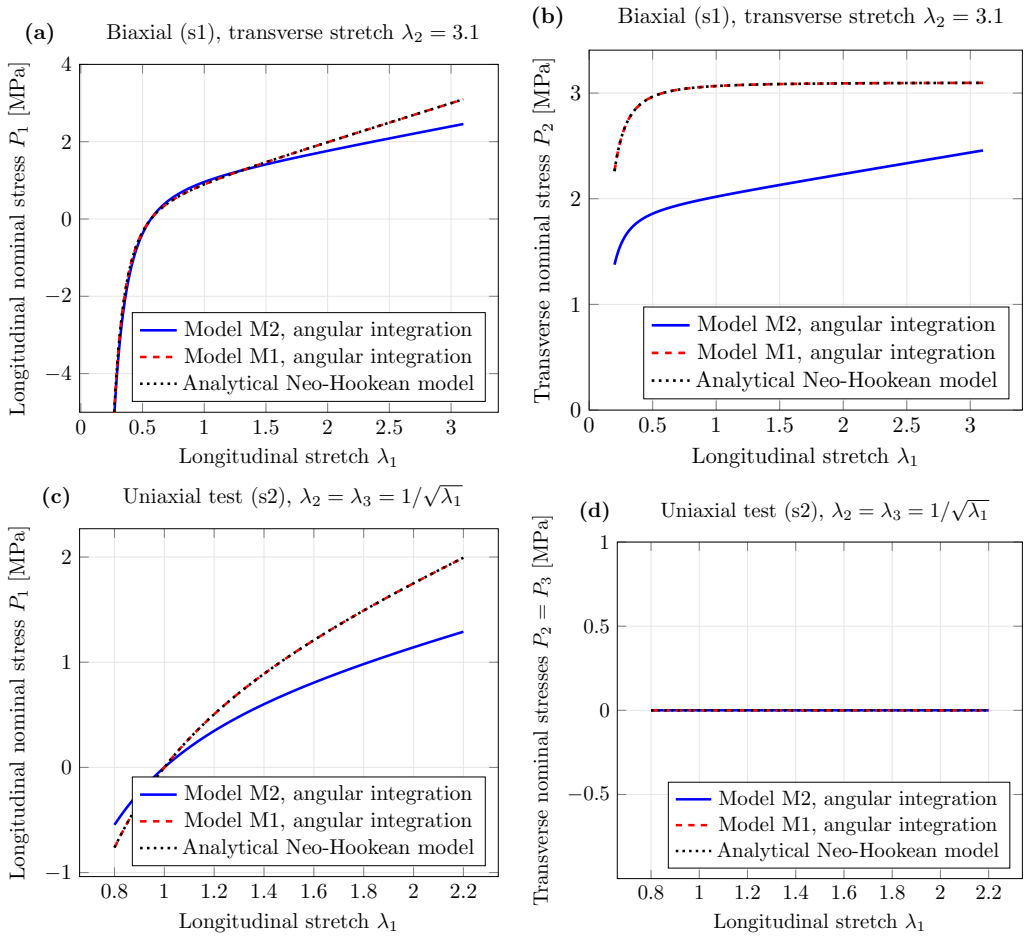

Figure 5: Relevance of different micro-macro connections through different chain stretches. Comparison of material behavior when using model M1 and model M2 through angular integrations, and the analytical Neo-Hookean model (equivalent to model M1). a) Biaxial test (s1) in which $\lambda_2 = 3.1$ is fixed and λ_1 varies; P_1 vs. λ_1. b) Cross-effect shown in P_2 vs. λ_1. c) Uniaxial test (s2) in axis 1; P_1 vs. λ_1. d) Transverse stresses $P_2 = P_3$ in the uniaxial test (s2) for $\lambda_2 = \lambda_3 = 1/\sqrt{\lambda_1}$, showing fulfillment of the incompressibility condition. Note that red dashed curves and black dotted curves are superimposed because the M1 model is the same as the classical Neo-Hookean model from the Gaussian network theory, see Sec. 4.2 of Treloar (1975)

As commented, expected, and observed in Fig. 5, model M1 integrated angularly is completely equivalent to the well-known Neo-Hookean model. Note that Fig. 5 also serves as a check of the accuracy of the numerical angular integration scheme employed. However, in that figure it can also be observed that the

behaviors of models M1 and M2 are substantially different, meaning that despite the resemblance of Eqs. (60) and (61) and that $\lambda_{ch} = \lambda_{ch}^C$ in principal directions of macroscopic deformation, the chain stretch variable used to link the chain behavior to that of the continuum has a substantial impact.

An interesting aspect of the Neo-Hookean model can be noted. For large stretches during a biaxial test with constant λ_2, we have that the transverse and the longitudinal moduli are

$$\frac{\partial P_2}{\partial \lambda_1} = \frac{2\mu}{\lambda_1^3 \lambda_2^3} \quad \text{and} \quad \frac{\partial P_1}{\partial \lambda_1} = \mu \left(1 + \frac{3}{\lambda_1^4 \lambda_2^2} \right) \tag{67}$$

The first one is interesting, because it shows that for moderate stretches and a constant modulus μ, the affine models show no appreciable increase in transverse stresses P_2 when the material is strained in the longitudinal direction. For example for stretches of, say, $\lambda_1 = \lambda_2 = 2$, we have $\partial P_2/\partial \lambda_1 = \mu/32$. This is the horizontal behavior observed in Fig. 5b for the Neo-Hookean model. A relevant positive slope could only be achieved for large stretches if the modulus μ has a strong increase, locking-type behavior. Note however that model $M2$ has a hardening in the transverse direction when the longitudinal one is stretched. The second one in Eq. (67) is that a constant μ means also a constant slope μ for large stretches. This can also be observed in Fig. 5b. These observations are interesting as a reference for analysing predictions of affine models during biaxial tests in real materials; see Sec. 5.

Note also that during a tensile test, the apparent Young modulus is different for both models, despite that resemblance. Indeed, a perturbation analysis shows that both moduli are related by a factor of 0.7, being 3μ the Neo-Hookean case. However, even when both uniaxial moduli are made equal (scaling μ of M2 by 1/0.7), the behaviour from both models is clearly different, see Fig. 6, because the physics behind both models is different. An interesting observation to which we will refer in Sec. 5 can also be made. In Fig. 6a both models have the same initial slopes (from the constant μ) for the uniaxial test, and they keep a large similitude for the quite large range shown. This results in also the same slopes ($\approx \mu$, see Eq. (67)) for the longitudinal curve $P_1 - \lambda_1$ for $\lambda_1 \gtrsim 1$, Fig. 6c; but note that whereas model M2 has a positive $P_2 - \lambda_1$ slope for the transverse behavior ($\lambda_1 \gtrsim 1$), Fig. 6d, the Neo-Hookean model gets an almost vanishing one, see Eq. (67). Remarkably, this means that the transverse tension in biaxial tests with a fixed transverse stretch ($\lambda_2 \gtrsim 1$) remains insensitive to longitudinal stretch increments (with $\lambda_1 \gtrsim 1$) already in the moderate tension ranges. This contradicts experimental observations (e.g. Table I in Rivlin and Saunders (1951); see also experiments of Kawabata et al. (1981); Kawamura et al. (2001) and Sec. 5), which show an increase of tension from transverse stretching in the order of $P_2/P_1 \approx 1/4$ (depending on the stretches), similar to that shown by model M2.

Moreover, another important observation is given in the Mooney plot for the tensile test shown in Fig. 6b. Mooney motivated his model $\Psi(I_1, I_2) = C_1(I_1 - 3) + C_2(I_2 - 3)$ in this type of plot, which for the uniaxial test results in

$$\frac{P_1}{2(\lambda_1 - 1/\lambda_1^2)} = C_1 + \frac{C_2}{\lambda_1} \tag{68}$$

In Mooney's model, the constants are $C_1 = \partial\Psi/\partial I_1$ and $C_2 = \partial\Psi/\partial I_2$. As mentioned in the Introduction Section (claim C0) the classical statistical theory does not predict any term in I_2, so in Mooney's plot it shows an horizontal line at Mooney's C_1 value of $C_1 = \mu/2$; see Fig. 6b. However, experiments in polymers consistently show a positive slope, which in view of Eq. (68), Mooney related to C_2. Using several types of tests, Rivlin and Saunders (1951) did a detailed experimental analysis of the ratios $(\partial\Psi/\partial I_2)/(\partial\Psi/\partial I_1)$, which is C_2/C_1 in Mooney's model. Rivlin and Saunders (1951) found a relation $(\partial\Psi/\partial I_2)/(\partial\Psi/\partial I_1) = 1/8$ for small stretches to 1/30 for large stretches. Whereas from experiments it is seen that $\partial\Psi/\partial I_2$ has a strong dependence on both I_1 and I_2 (it decreases for increasing values of the invariants), the 1/6 to 1/30 are values in the order of the slope of Fig. 6b. However, Rivlin and Saunders (1951) and Obata et al. (1970) warned about Mooney's simplistic interpretation of the almost straight slope as a validation of Mooney's model, because at small stretches, experiments show also a relevant dependence of $\partial\Psi/\partial I_1$ with deformation; see detailed discussion in (Treloar, 1975, Ch.10). In this line, we must remark that the Mooney-Rivlin invariants where developed from the apparition of I_1 in the Gaussian-Neo-Hookean (affine) theory ($I2$ has been introduced to handle the "small deviations"), but model M2 is not based on such invariants, so we should not expect a simple expression in terms of I_1 and I_2.

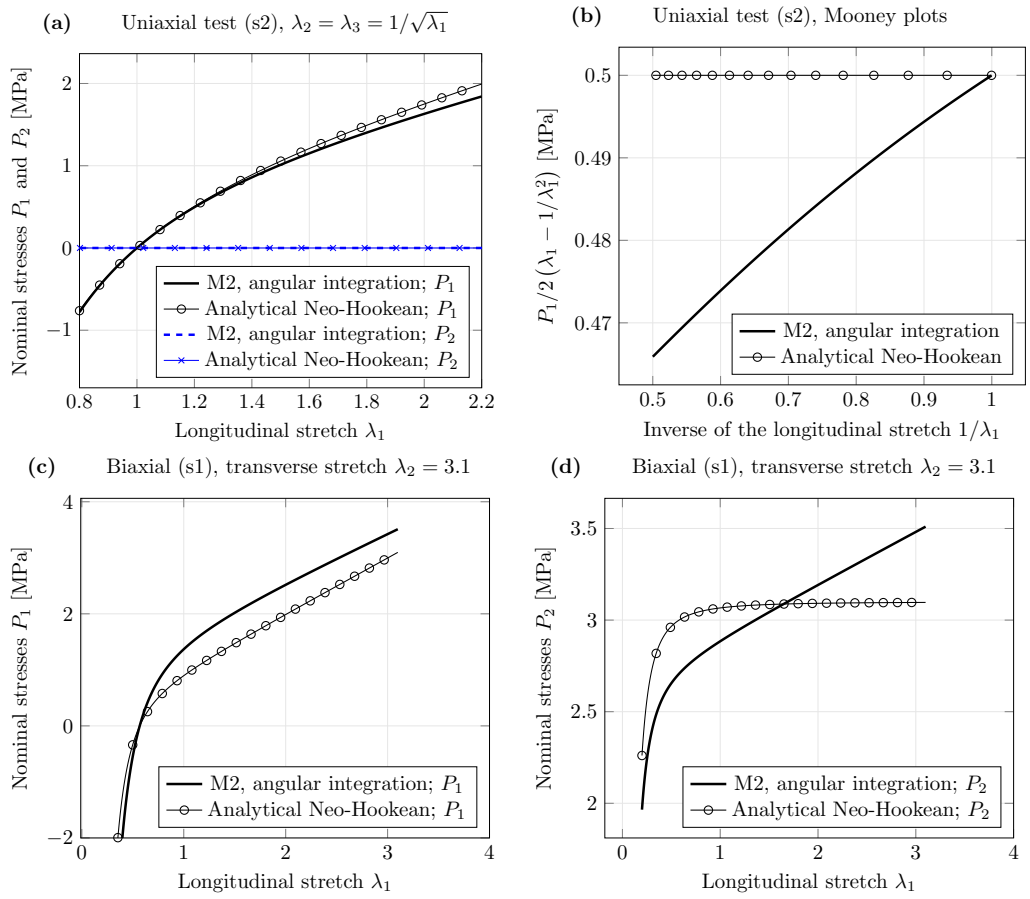

Figure 6: Comparison of material behavior when using model M2 through angular integrations with scaled modulus $\mu^* = \mu/0.7$ and the analytical Neo-Hookean model (equivalent to model M1). a) Uniaxial test (s2) in axis 1; P_1 vs. λ_1 and P_2 vs. λ_1. b) Uniaxial test (s2) Mooney plots. c) biaxial test (s1) in which $\lambda_2 = 3.1$ is fixed and λ_1 varies; P_1 vs. λ_1. d) biaxial test (s1) in which $\lambda_2 = 3.1$ is fixed and λ_1 varies; P_2 vs. λ_1.

As a conclusion of this subsection, the Neo-Hookean model (hence model M1) is widely accepted to represent the behaviour of polymers at moderate stretches, those under which the Gaussian treatment is a good approximation. As most polymer network models, it uses two *fundamental assumptions* (cf. Treloar (1975) Sec. 4.2, pp. 60-61, assumptions #4 and #5): (a1) affine deformations in the network (chain junction points move embedded in the continuum, so the change of length in the chains is that of the line segment in the continuum); (a2) the entropy of the network is just the sum of the entropies of the individual chains (so the network configurational entropy due to the non-isotropic distribution of the orientations of the chains from the affinity constraint, Secs. 2.3 and 2.5, is neglected). In contrast, model M2 brakes these assumptions, replacing them by: (Ra1) the network is free to fluctuate, the same way as the links in the polymer chain; (Ra2) there is no constraint to establish the orientation of the chains, meaning that chains will remain isotropically oriented. The latter assumptions seem to include a proper dependence in I_2 in the statistical theory (Claim C0 in the Introduction), and comply better with experimental observations.

4.2. The macro-micro-macro approach using different micro-macro connections

In Amores et al. (2020) we presented a Macro-Micro-Macro (MMM) approach to model polymers. The approach is an extension of WYPiWYG hyperelasticity (Sussman and Bathe (2008); Crespo et al. (2017); Latorre and Montáns (2014)) to travel scales to reverse-engineer the chain behavior in a polymer from a single experimental test (e.g. a tensile test). Once that average chain behavior is obtained, it may be employed to simulate the behavior of the polymer under any (homogeneous or non-homogeneous) loading condition, either through angular integration or, more efficiently, through pre-computed constitutive manifolds, see Amores et al. (2020).

The MMM approach is quite general and simply hinges in a proper description of the microstructure of the material and its micro-macro connection. In Amores et al. (2020) we employed the same network layout and micro-macro connection as in model M2, namely

$$\Psi^{(2)}(\lambda_1,\lambda_2,\lambda_3)=\frac{1}{\Omega}\int_\Omega \psi_{ch}^{(2)}(\lambda_{ch})d\Omega \tag{69}$$

However, the same procedure may be applied employing the assumptions in model M1, namely

$$\Psi^{(1)}(\lambda_1,\lambda_2,\lambda_3)=\frac{1}{\Omega}\int_\Omega \psi_{ch}^{(1)}(\Lambda_{ch})d\Omega \tag{70}$$

We emphasize that with either assumption Eq. (69) or Eq. (70), the respective chain energy function (the unknown function) may be obtained using the MMM procedure *from a single test* (the known function) and that the chain behavior will be such that the presented test will be captured exactly if desired (numerically speaking) as happens with all WYPiWYG procedures. Importantly, of course it does not mean that we will be able to capture the behavior of the material under any loading condition. The accuracy of such simulations will be parallel to the accuracy of the micro-macro description of the model, i.e. whether the assumptions (a1), (a2), (Ra1), (Ra2) are accurate. In Fig. 7 we show this observation. In that figure we use the "experimental" data from the analytical Neo-Hookean model for a biaxial test with a fixed $\lambda_2=3.1$ in axis 2, and a varying λ_1 in axis 1. It is seen in Fig. 7a that both MMM models capture accurately such behavior, but the corresponding chain functions shown in Fig. 7b (plotted in comparable squared stretches, modulus alike) are clearly different. Furthermore, having captured the test in Fig. 7a means little about having characterized the actual behavior of the material under general deformations, as the transverse stresses in Fig. 7c and the stresses for a uniaxial test in Fig. 7d show.

Of course a minimum squares approach with several tests may be employed as typically done in determining material parameters of polymer models; overall better predictions will be obtained for the tests, but model MMM (2) will never be capable of capturing the Neo-Hookean model because the intrinsic structure of the model (i.e. assumptions (a1) and (a2)) are different.

At this point it should be evident to the reader that the opposite also holds. If we try to capture model M2, Eq. (61), with the MMM approach using Λ_{ch}, Eq. (70), we will be uncapable of obtaining satisfactory results. This observation is summarized in Fig. 8.

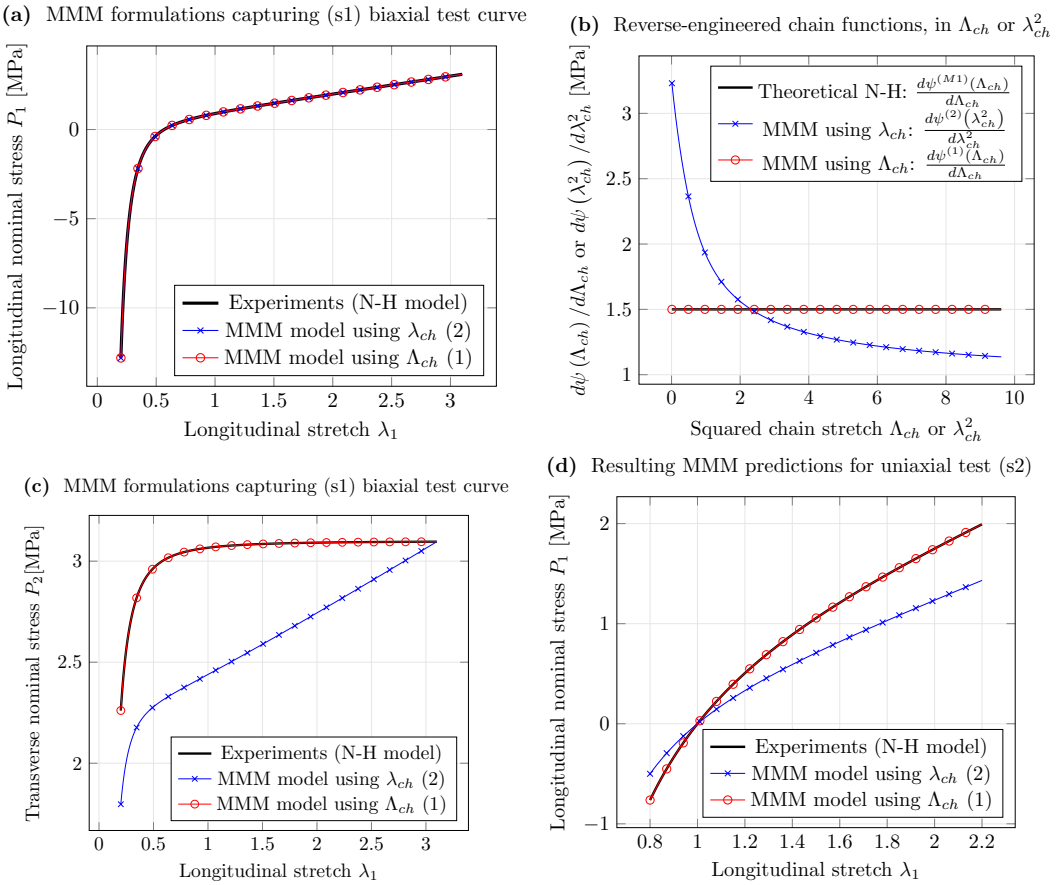

Figure 7: Macro-Micro-Macro reverse engineering of the Neo-Hookean model using only "experimental" data from a biaxial test with fixed $\lambda_2 = 3.1$ and varying λ_1. The two microstructural assumptions are employed in the MMM approach: (1) affine network deformations using $\Lambda_{ch} = \boldsymbol{C} : \hat{\boldsymbol{r}} \otimes \hat{\boldsymbol{r}}$; and (2) free network using $\lambda_{ch} = \boldsymbol{U} : \hat{\boldsymbol{r}} \otimes \hat{\boldsymbol{r}}$. a) Resulting predictions for the test employing to characterize the model (determine the chain function); note that both approaches capture exactly (numerically speaking) the prescribed test data. b) Reverse-engineered chain functions, compared to the theoretical Neo-Hookean one from which "experimental" data has been obtained; note that they are plotted in terms of squared stretches (modulus alike), namely $d\psi/d\lambda_{ch} = 2\lambda_{ch} d\psi/d\lambda_{ch}^2$ is an increasing function. c) Theoretical and predicted transverse nominal stresses for the (s1) test; note that, as expected, the MMM model (1) also captures accurately the behavior, but the MMM model (2) fails to do so despite capturing exactly the behavior in the other axis. d) Predictions of both models with the captured chain functions for a different test: the uniaxial test; a similar conclusion is obtained as for case c).

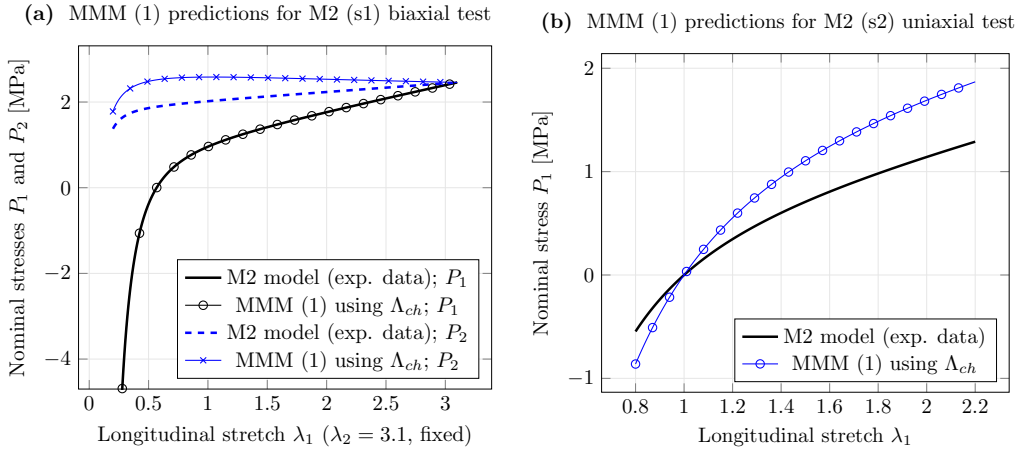

Figure 8: Reverse engineering of the M1 model of Eq. (61) using the MMM approach with Λ_{ch} (affine assumption). For all the plots in this figure, the MMM model is also calibrated from the $P_1 - \lambda_1$ curve of the biaxial (s1) test (with $\lambda_2 = 3.1$ fixed). a) Predictions for the biaxial test (s1), both longitudinal P_1 and transverse P_2 nominal stresses. b) Predictions for the uniaxial (s2) test.

As a conclusion of this subsection to keep in mind for the next section, the MMM approach is capable of accurately capturing the chain behavior of a material if that material behaves according to the assumptions employed in the MMM formulation, but fails to give reasonably accurate results if these assumptions do not hold.

5. Comparison of assumptions against experimental data in polymers

With the observations from the previous section, to capture experimental data of actual polymer materials we now employ the MMM method using both assumptions: unconstrained isotropic network configuration (use of λ_{ch}) and constrained affinely oriented chains (use of Λ_{ch}). The experimental data used for this study are the true biaxial family of tests from Kawabata et al. (1981). This material is almost identical to that from Treloar (1944) (same composition of unfilled cross-linked rubber with 8ph sulfur, and very close experimental results for uniaxial, equibiaxial and pure shear tests), whose experiments are used in most works to test the predictive power of material models. Remarkably, Kawabata et al. (1981) experiments are complete for an incompressible material, because they are true biaxial tests in which both λ_1 and λ_2 are prescribed independently ($\lambda_3 = 1/(\lambda_1\lambda_2)$, so in those experimental sets all possible states of deformation are tested (obviously within the experimental range of deformations). Hence, if a model is capable of accurately predicting the behavior of all Kawabata et al. (1981) sets of experiments we can claim that the model represents accurately the material behaviour under any loading condition.

We first address the characterization of the chain function *using a single test curve*, namely the curve for fixed $\lambda_2 = 3.1$ and varying λ_1. This curve consists of *just* the *seven experimental points* shown in Fig. 9a. With these seven experimental points (interpolated through the B-spline also shown in Fig. 9a), using the MMM method (Amores et al., 2020), we reverse-engineer the chain function $d\psi_{ch}/d\lambda_{ch}$, a result shown in Fig. 9b. With this chain function, via angular integration, we predict all the tests from Kawabata et al. (1981) both the longitudinal stress P_1 and the transverse stress P_2, and for both the small stretch range and the large stretch range. Figure 10 shows the comparison of the predictions against experimental data. Remarkably, from just the mentioned seven experimental points used to characterize the material, we are capable of accurately predicting the behavior of the material under any loading condition. Indeed, this accuracy does not only hold for the Kawabata et al. (1981) material: similar accuracy has been obtained for different types of silicones tested also through true biaxial tests by Kawamura et al. (2001); see predictions in Amores et al. (2020). We have used 21 quadrature points as in Bazant and Oh (1986), but we note

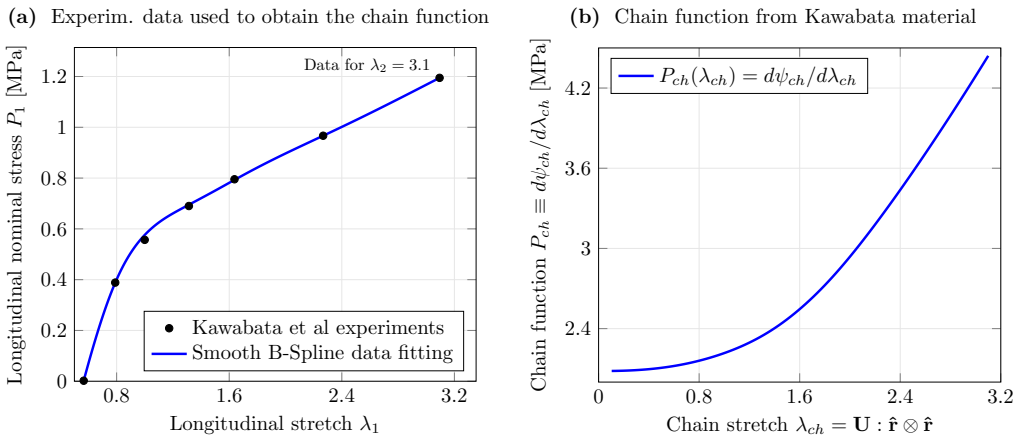

Figure 9: Reverse-engineering of the chain function from Kawabata et al material. (a) Experimental data from Kawabata et al for $\lambda_2 = 3.1$ employed in the determination of the chain function, and smooth spline to interpolate experimental data in the MMM procedure; only these data from a single test curve have been employed to obtain the chain function. (b) Resulting chain function for the Kawabata material under the assumption of isotropic chain distribution during deformation (non-affine, unconstrained orientation of network chains)

that in our case no relevant difference is appreciated when using other more intensive quadrature rules, see discussion in Amores et al. (2020).

From Fig. 10 we can conclude that the assumption of unconstrained network chain orientations, or equivalently the use of $\lambda_{ch} = \boldsymbol{U} : \hat{\boldsymbol{r}} \otimes \hat{\boldsymbol{r}}$ as state variable to determine the chain stretch, seems adequate to describe the polymer behavior under general state of deformations. However, one may question that the predictive capability may de attributed to the MMM approach and its suitability to reverse-engineer the chain behavior, and not to the mentioned assumption. To verify this, we have also employed the MMM approach using the affinity assumption for the orientation of the network chains; equivalently Λ_{ch}. Following the same procedure, with the same seven mentioned experimental points and with the same interpolating B-spline, we reverse-engineered the chain function $d\psi_{ch}(\lambda_{ch}^C)/d\lambda_{ch}^C$. With that chain function, via angular integration, we performed the predictions for the Kawabata et al. (1981) experiments. This comparison is shown in Fig. 11. It is observed that the MMM model using the affinity assumption gives large errors, except for the $P_1 - \lambda_1$ curve with $\lambda_2 = 3.1$ which is indeed the curve employed to characterize the material. As in Fig. 7, the prediction for the equibiaxial test at $\lambda_1 = \lambda_2 = 3.1$ is accurate for both P_1 and P_2 (in plane chain orientations in this case are isotropic for both models, and the materials behave isotropically). From the conclusions of Sec. 4.2, the MMM model can only capture the behavior of a polymer under any loading conditions if the micro-macro assumptions represent properly the actual behavior, so the comparison of Figs. 10 and 11 seem to favor the unconstrained (non-affine, isotropic) chain orientations in the network. Moreover, it is interesting to compare the shape of Fig. 9a (reproduced now by both MMM approaches accurately) to that of the $P_1 - \lambda_1$ curves in Fig. 6b for $\lambda_1 \gtrsim 1$: they have an almost constant slope. Recalling the comments regarding the slopes of transverse curves $P_2 - \lambda_1$, the affine model resulted in a vanishing slope, whereas the non-affine one maintained a possitive slope. Note that the transverse *experimental* data $P_2 - \lambda_1$ in Fig. 10c has a positive (almost constant) slope, easily accomodated by the non-affine model. In contrast, the affine model results in a negative slope for that curve.

However, even though sometimes questioned, the affine deformations approach has been employed by many researches in a large amount of material models for almost a century. Albeit not accurate, somewhat reasonable predictions using this assumption have been obtained for many materials, including the Kawabata et al material, so the results in Fig. 11 seem to contradict the vast experience using the affinity assumption. The poor results in Fig. 11 could be attributed, for example, to inadequacy of the MMM approach or to the lack of sophistication in the model. Such type of sophistication includes, for example, constraining tubes for chains (changing the assigned surface) or the non-affinity in the chain stretch (free fluctuating field as in the

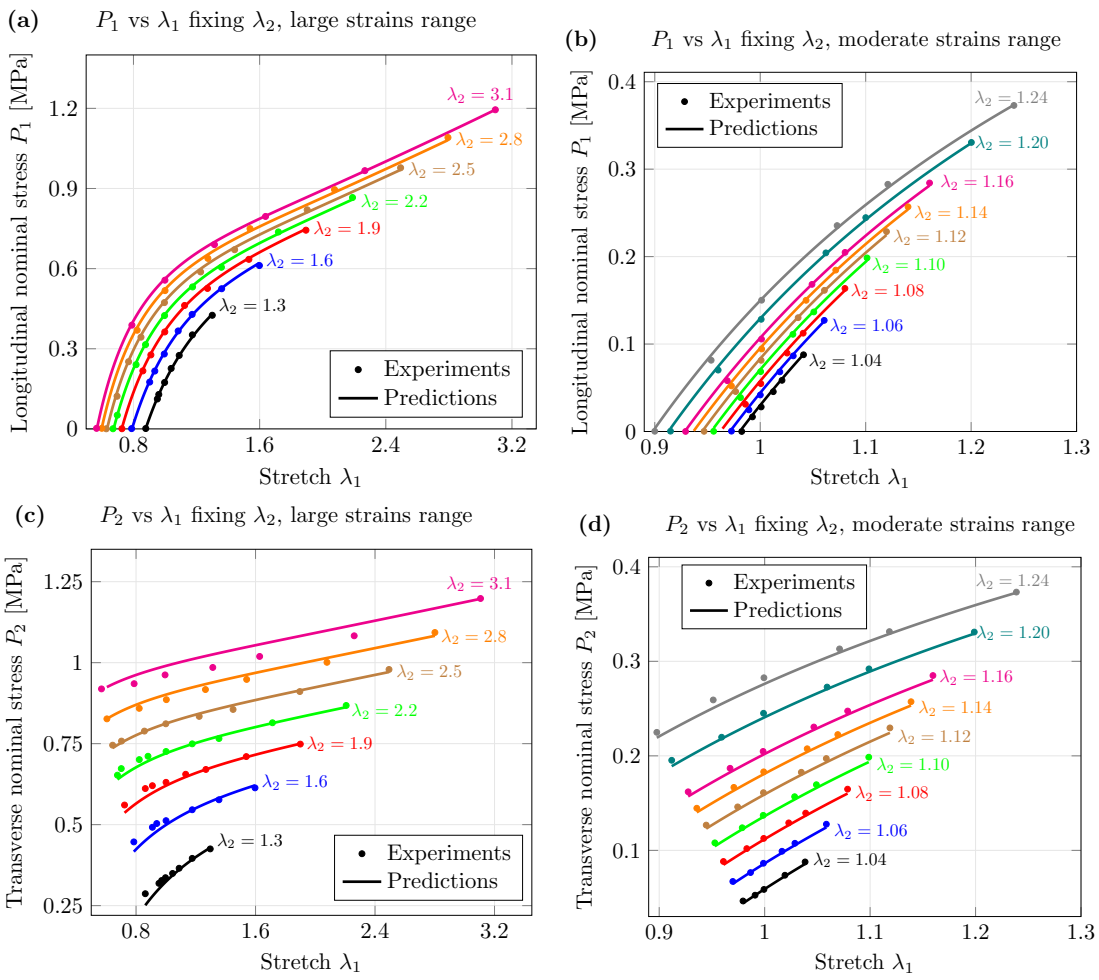

Figure 10: Predictions of the Kawabata et al biaxial experiments Kawabata et al. (1981) using the present macro-micro-macro proposal *under the non-affine orientational assumption*, where $P_{ch}(\lambda_{ch})$ has been characterized from the $P_1(\lambda_1)$ curve for $\lambda_2 = 3.1$. Dots represent experimental data, whereas continuous curves represent the predictions. (a) Longitudinal nominal stresses P_1 as a function of the longitudinal stretch λ_1 for different fixed values of the transverse stretch λ_2; large stretches range. (b) Longitudinal nominal stresses P_1 as a function of the longitudinal stretch λ_1 for different fixed values of the transverse stretch λ_2; moderate stretches range, shown in a different plot for legibility. (c) Transverse nominal stresses P_2 as a function of the longitudinal stretch λ_1 for different fixed values of the transverse stretch λ_2; large stretches range. (d) Transverse nominal stresses P_2 as a function of the longitudinal stretch λ_1 for different fixed values of the transverse stretch λ_2; moderate stretches range, shown in a different plot for legibility.

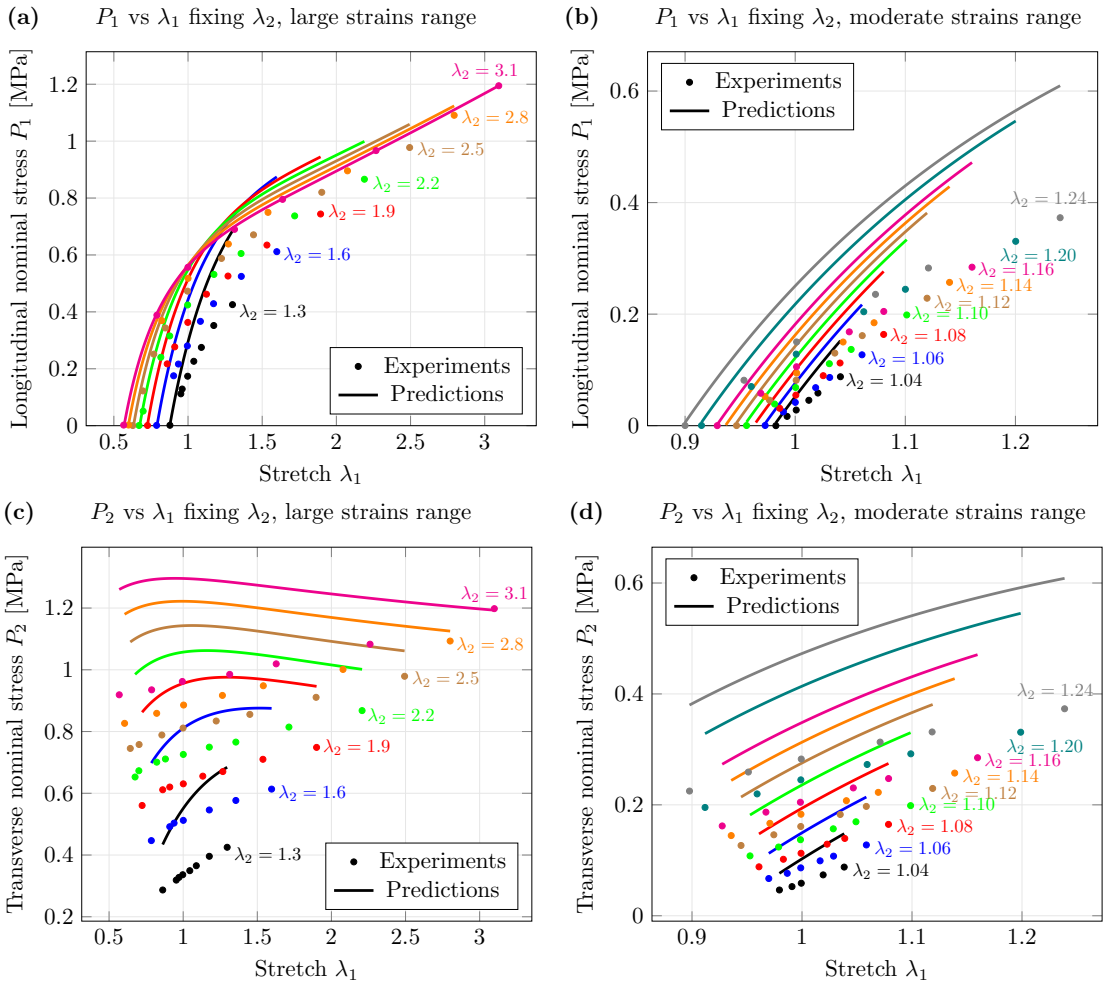

Figure 11: Predictions of the Kawabata et al biaxial experiments Kawabata et al. (1981) using the present macro-micro-macro proposal *under the affine orientational assumption*, where the chain function $P_{ch}(\lambda_{ch}^C)$ has been characterized from the $P_1(\lambda_1)$ curve for $\lambda_2 = 3.1$. Dots represent experimental data, whereas continuous curves represent the predictions. (a) Longitudinal nominal stresses P_2 as a function of the longitudinal stretch λ_1 for different fixed values of the transverse stretch λ_2; large stretches range. (b) Longitudinal nominal stresses P_1 as a function of the longitudinal stretch λ_1 for different fixed values of the transverse stretch λ_2; moderate stretches range, shown in a different plot for legibility. (c) Transverse nominal stresses P_2 as a function of the longitudinal stretch λ_1 for different fixed values of the transverse stretch λ_2; large stretches range. (d) Transverse nominal stresses P_2 as a function of the longitudinal stretch λ_1 for different fixed values of the transverse stretch λ_2; moderate stretches range, shown in a different plot for legibility.

microsphere model), among others. The qualitative observations regarding slopes could also be attributed to the limit in the validity of the Gaussian theory.

To further investigate the reason behind the poor predictions in Fig. 11, we have repeated the process employing in this case the uniaxial tension-compression test data from Kawabata et al. (1981) to reverse-engineer the chain function of the affine model. The data corresponding to the Kawabata uniaxial test, is extracted from the same set experiments given in Fig. 11. The predictions of the Kawabata et al. (1981) experiments using the new chain function determined using the uniaxial data, are given in Fig. 12.

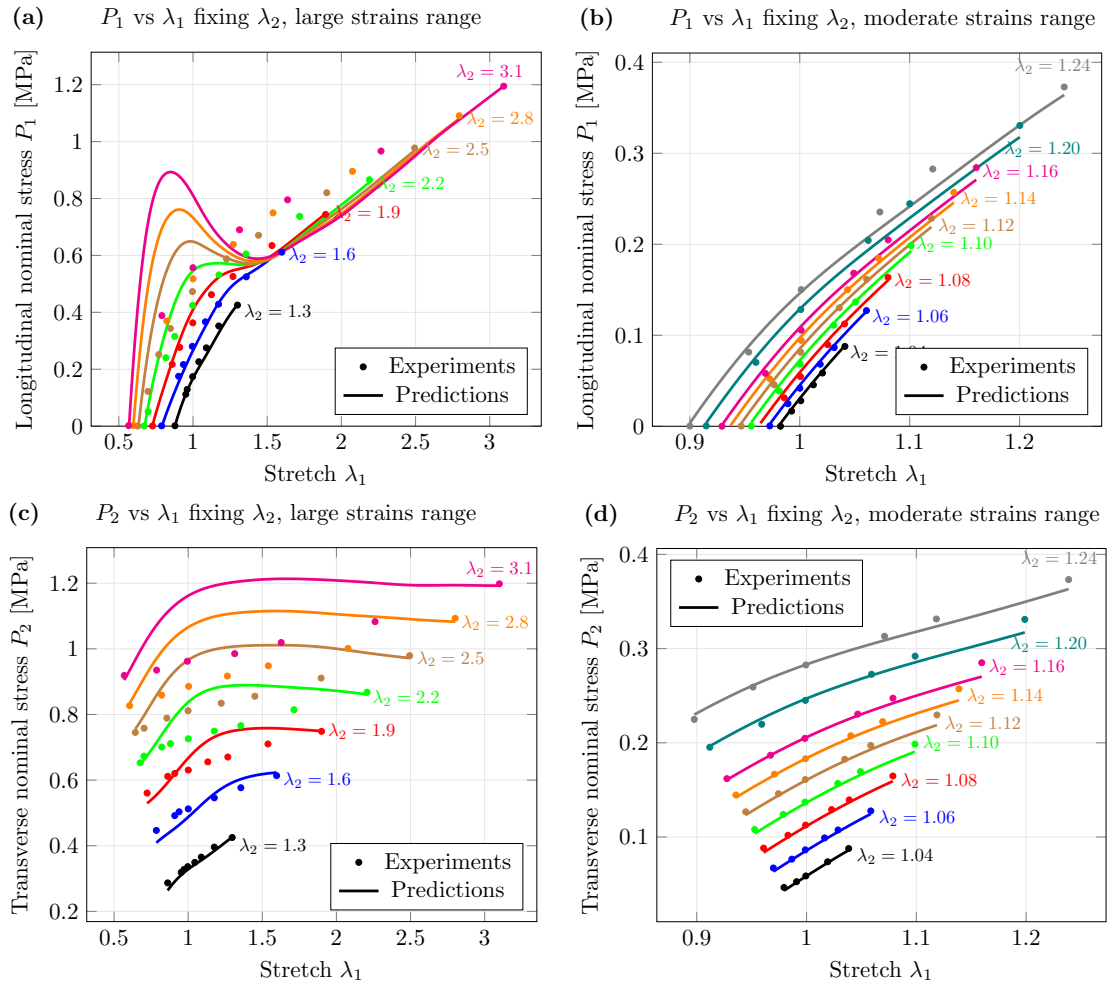

Figure 12: Predictions of the Kawabata et al biaxial experiments Kawabata et al. (1981) using the present macro-micro-macro proposal *under the affine orientational assumption*, where the chain function $P_{ch}(\lambda_{ch}^C)$, where the chain function has been characterized from the uniaxial test. Dots represent experimental data, whereas continuous curves represent the predictions. (a) Longitudinal nominal stresses P_1 as a function of the longitudinal stretch λ_1 for different fixed values of the transverse stretch λ_2; large stretches range. (b) Longitudinal nominal stresses P_1 as a function of the longitudinal stretch λ_1 for different fixed values of the transverse stretch λ_2; moderate stretches range, shown in a different plot for legibility. (c) Transverse nominal stresses P_2 as a function of the longitudinal stretch λ_1 for different fixed values of the transverse stretch λ_2; large stretches range. (d) Transverse nominal stresses P_2 as a function of the longitudinal stretch λ_1 for different fixed values of the transverse stretch λ_2; moderate stretches range, shown in a different plot for legibility.

These plots show better results than those in Fig. 11. However, it is observed that the good accuracy is obtained only for small-to-moderate stretches, being predictions for large stretches disappointing. Furthermore, the observation regarding the slopes still holds. Note that now both ends of the curves are prescribed in the process (they correspond to the prescribed B-spline from uniaxial tension-compression or

tensile-equibiaxial tests), so the model tries to comply with that data, whatever the resulting chain function is. Our explanation to the improved results of Fig. 12 over Fig. 11 comes from the configuration from which the chain function has been reverse-engineered. The uniaxial test departs from an unloading configuration. In that configuration the affinity assumption has an isotropic network distribution of chains, so no conclusion may be extracted regarding the accuracy of either assumption. Only at large stretches the distribution becomes strongly anisotropic (specially during the tensile test). Then, when the chain function is reverse-engineered from a tensile test, moderate strain results will be very similar under both orientational assumptions, but at very large strains, differences in orientational distributions are significative, see Fig. 3e, so are the differences between both models. These comments are indeed behind the reason of using the biaxial test curve with a fixed $\lambda_2 = 3.1$ and variable λ_1 to reverse-engineer the chain function in the paper. For this test curve the orientational distribution of the chains for the affine assumption is strongly anisotropic, so if this curve is used, differences between both approaches are emphasized. This observation may be in connection with the Miehe et al. (2004) claim quoted as (C2) in Sec. 1 regarding the need for the non-affine correction to λ_{ch}^C especially in the range of large deformations.

We recall that, to date, no micromechanical model under the assumption of affine orientation of chains has been capable of reproducing accurately all the tests of the Kawabata et al. (1981) material (or similar polymer) using only one test curve to characterize the model. When using several test curves to characterize the chain behavior (material parameters), as done in Markmann and Verron (2006), the different orientational distributions from the tests are somehow implicitly averaged, so the resulting chain function performs better over all ranges of deformations than when using a single one. However, this does not validate any assumption on the microstructural arrangement of the chains, because for example, Ogden's phenomenological model (Ogden, 1972) gives similar or better performance using just two tests (Latorre et al., 2017a; Ogden et al., 2004). For this reason, it is widely used to characterize polymeric materials and available in most finite element codes. Indeed, as mentioned in the Introduction Section, Ogden's and Shariff's (Shariff, 2000) models, both phenomenological models based in the Valanis and Landel (1967) decomposition, where best performers in the comparison made by Markmann and Verron (2006) for predicting the Kawabata et al. (1981) experiments. For example, the results shown in Fig. 3 of Markmann and Verron (2006) look marginally better than those using the Miehe et al. (2004) microsphere model (Fig. 8 in Markmann and Verron (2006)); compare also Figs. 4, 11-13 of Kiêm and Itskov (2016).

The excellent performance of Ogden's and Shariff's models deserves some study here. These models are based on the Valanis and Landel (1967) decomposition:

$$\Psi(\lambda_1, \lambda_2, \lambda_3) = \omega(\lambda_1) + \omega(\lambda_2) + \omega(\lambda_3) \tag{71}$$

where $\omega(\lambda) = \sum_{k=1}^{\infty}(\mu_k/\alpha_k)(\lambda^{\alpha_k} - 1)$ is the particular fitting function chosen by Ogden; Shariff's model just changes the fitting function. Valanis and Landel already made an assessment of the decomposition using several types of tests concluding its suitability for a moderately large range of stretches (see additional validations in Obata et al. (1970); Treloar (1975)). The same Valanis and Landel (1967) decomposition has been used in the WYPiWYG models (Sussman and Bathe, 2008; Crespo et al., 2017; Latorre et al., 2017a; Ogden et al., 2004), where the function $\omega(\lambda)$ is obtained in spline form, with a numerically exact fit just employing the Kearsley and Zapas (1980) series or solving a system of equations.

Emphasis in using as many tests as possible in fitting parameters of models is continuously placed in the literature e.g. Pancheri and Dorfmann (2014); Markmann and Verron (2006); Ogden et al. (2004); Criscione (2003); Kiêm and Itskov (2016); Urayama (2006); claim (C3) in Sec. 1. However, we can consider Valanis-Landel models as three-chain models, whose chains are aligned with the principal directions of deformation. The weight for each chain is $4\pi/3$. Indeed, the model is also the same as an angularly integrated model in which only three integration points are used. The direction vectors of those integration points are $\hat{\boldsymbol{n}}_i$, the principal directions of deformation. Then, we can apply our MMM method, with just 3 integration points, to obtain the chain function for this model in the same way as we did before. We use once again the same 7 experimental points from the $P_1 - \lambda_1$ curve with $\lambda_2 = 3.1$ to reverse-engineer the chain function $P_{ch}(\lambda_{ch}) = 3/(4\pi)\omega'(\lambda)$. With this chain function, we repeat the predictions for the Kawabata et al. (1981) experiments using this "three-chain" model. The results are shown in Fig. 13.

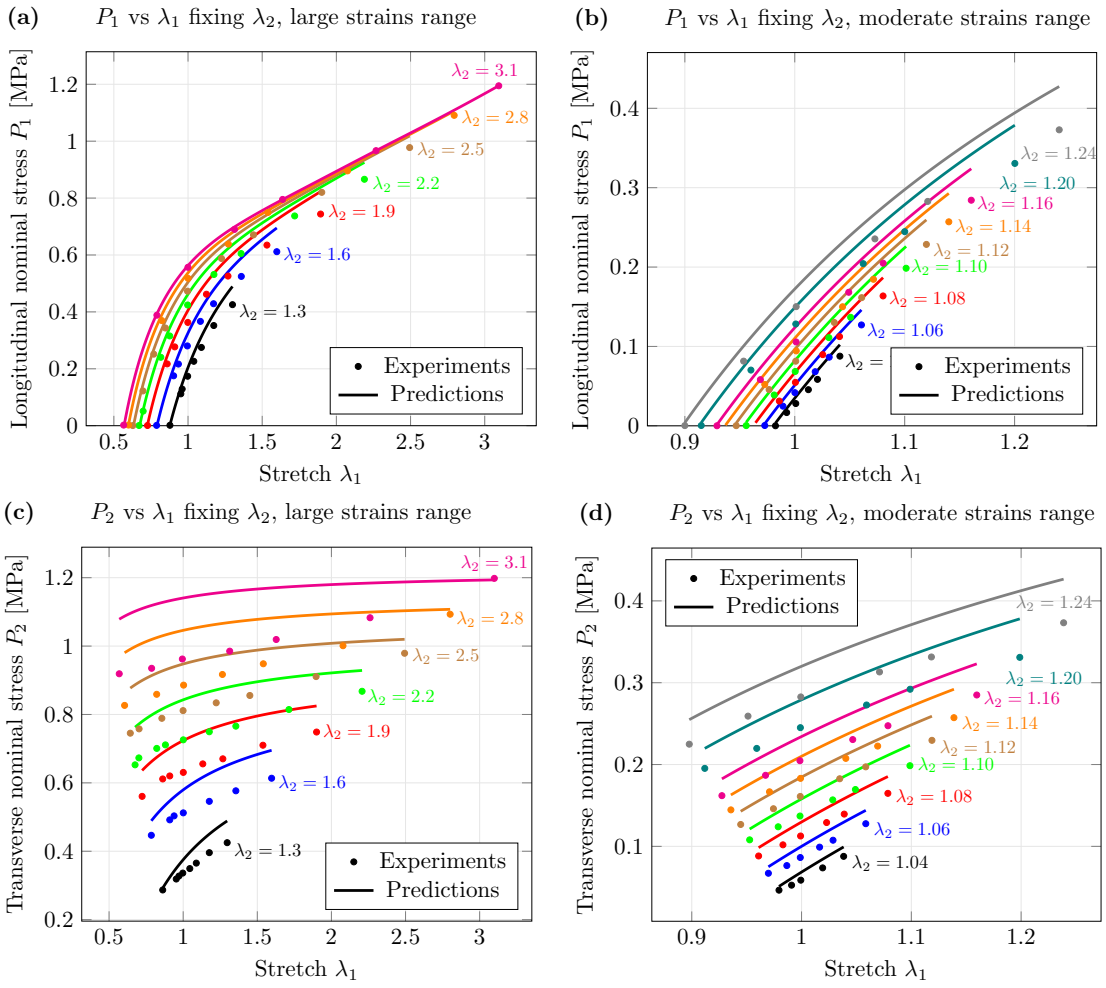

Figure 13: Predictions of the Kawabata et al biaxial experiments Kawabata et al. (1981) using the present macro-micro-macro proposal *with only three integration points oriented at the principal continuum deformation directions*, where $P_{ch}(\lambda_{ch})$ has been characterized from the $P_1(\lambda_1)$ curve for $\lambda_2 = 3.1$. Dots represent experimental data, whereas continuous curves represent the predictions. (a) Longitudinal nominal stresses P_1 as a function of the longitudinal stretch λ_1 for different fixed values of the transverse stretch λ_2; large stretches range. (b) Longitudinal nominal stresses P_2 as a function of the longitudinal stretch λ_1 for different fixed values of the transverse stretch λ_2; moderate stretches range, shown in a different plot for legibility. (c) Transverse nominal stresses P_2 as a function of the longitudinal stretch λ_1 for different fixed values of the transverse stretch λ_2; large stretches range. (d) Transverse nominal stresses P_2 as a function of the longitudinal stretch λ_1 for different fixed values of the transverse stretch λ_2; moderate stretches range, shown in a different plot for legibility.

Interestingly, despite using only one test curve, the same that resulted in poor predictions for the affine model, the predictions for this three chain model are rather good in both P_1 and P_2, and in both the low stretch and large stretch ranges, with maximum errors of about 20% and keeping the tendencies of the experimental curves. Indeed, Fig. 13a may be compared with the results of the 8-chain model in Fig. 6 of Markmann and Verron (2006). Whereas the 8-chain model gives good predictions for the low stretch region, it fails to give reasonable predictions for the true biaxial tests in the large stretch region, despite capturing simultaneously a tensile test and an equibiaxial test rather well, as Fig. 6 of Markmann and Verron (2006) shows. Hence, this may be an explanation of the success of both the Ogden and the Shariff models.

However, the predictions in Fig. 13 are much more interesting if they are compared to those given in Figs. 10 and 11. For computing the 3-chain model in Fig. 13 we have not specified whether we used the affinity assumption or not, simply because in this 3-chain model both assumptions are essentially the same because the three chains are aligned with the principal directions of deformation (for these three chains in the model $\lambda_{ch}^2 = \Lambda_{ch}$). Then, Fig. 10 may be seen as the improvement over Fig. 13 when more chains (or integration points) are included in the model following the unconstrained network assumption. In contrast, Fig. 11 may be seen as the improvement over Fig. 13 when more chains (or integration points) are included in the model following the affine assumption. From the comparisons, it is clear that in the first case the results improve as expected, but in the second case, including more chains worsens the accuracy. This is in line with the observations respect to the affine full network model (claim C1 in the Introduction).

6. Conclusions

In this paper we questioned the network affinity assumption in polymers respect to the orientational distribution of the chains during deformations. This assumption is tied to the use of the stretch from the right Cauchy-Green deformation tensor as the basic state variable (the micro-stretch) in the chain. These ingredients are employed by most polymer network and soft tissue models.

We have addressed the network configurational entropy to be added to the entropy of the individual chains. We observed that the affinity assumption introduces an additional stress if the changes of entropy due to such assumption are considered. This additional stress is typically neglected.

We have shown that the use of an unconstrained configuration assumption, in line with a negligible network configuration stress, results in an isotropic distribution of the orientation of chains during deformation. This average orientation of the chains is equivalent to employing the chain-projected stretch from the stretch tensor as the state variable for the stretch function. In contrast, the affinity assumption employs the chain-projected stretch from the Cauchy-Green deformation tensor.

We also have shown that both assumptions result, in general, in very different predictions for moderate-to-large stretches, and discussed long-standing issues regarding the absence of I_2 terms in the classical statistical theory which contradicts experimental observations. These terms are implicit in the proposed unconstrained formulation.

We have employed our recent data-driven macro-micro-macro approach to reverse-engineer the chain behavior from a single test curve using both assumptions, and have compared the predictions for the true biaxial test series from Kawabata et al. (1981). When using the unconstrained assumption and any single test curve to calibrate the material, we are capable of accurately predicting the behavior of the polymer for all tests. We have not been capable of doing so using the affinity assumption. Moreover, in our investigations, when the orientation of chains play a relevant role in the predictions, the network affinity assumption deviates more from experimental results. We are not aware of any model using this assumption capable of accurately capturing Kawabata's experiments (or any similar set) using only one test curve for obtaining the material parameters. However, we did so without including any additional ingredients like chain tube constraints or minimizing free-fluctuating chain stretch fields. Indeed, we have made connections with the different observations in the literature which highlight difficulties in predicting experimental results and which justified needed improvements.

Probably, the free orientational network assumption has also some range of validity which needs to be studied. The chain rotations and their stretches are coupled and both entropy contributions may have a

different balance in different cases, as it is apparently the case in collagenous tissues. Whether the changes in the network orientational entropy may be always neglected in isotropic polymers is an open question, but it seems probable that strongly crosslinked and swollen polymers may behave in an orientational more affine manner. That may also hold near chain locking stretches.

In summary, in our opinion, the assumptions behind the chain orientations in polymer networks during finite deformations should not be overlooked, because they have an important impact in the predictions and, hence, also in conclusions regarding the microstructure if these are just supported on the accuracy of predictions.

Acknowledgements

Partial financial support for the present work has been facilitated by the Agencia Estatal de Investigación, Ministerio de Ciencia, Innovación y Universidades of Spain, under grant PGC-2018-097257-B-C32.

References

Alastrué, V., Martínez, M., Doblaré, M., Menzel, A., 2009. Anisotropic micro-sphere-based finite elasticity applied to blood vessel modelling. Journal of the Mechanics and Physics of Solids 57, 178–203.

Amores, V., Benítez, J., Montáns, F., 2020. Data-driven, structure-based hyperelastic manifolds: A macro-micro-macro approach to reverse-engineer the chain behavior and perform efficient simulations of polymers. Computers and Structures 231, 106209.

Anthony, R.L., Caston, R.H., Guth, E., 1942. Equations of state for natural and synthetic rubber-like materials. I. Unaccelerated natural soft rubber. The Journal of Physical Chemistry 46, 826–840.

Argon, A., 2013. The physics of deformation and fracture of polymers. Cambridge University Presss.

Arruda, E., Boyce, M., 1993. A three-dimensional constitutive model for the large stretch behavior of rubber elastic materials. Journal of the Mechanics and Physics of Solids 41, 389–412.

Arruda, E., Boyce, M., 2000. Constitutive models of rubber elasticity: A review. Rubber Chemistry and Technology 73, 504–522.

Ball, R., Doi, M., Edwards, S., Warner, M., 1981. Elasticity of entangled networks. Polymer 22, 1010–1018.

Bazant, Z., Oh, B., 1986. Efficient numerical integration on the surface of a sphere. ZAMM-Journal of Applied Mathematics and Mechanics / Zeitschrift für Angewande Mathematik unk Mechanik 66, 37–49.

Bergström, J., 2015. Mechanics of Solid Polymers. Elsevier, Amsterdam.

Billiar, K., Sacks, M., 1997. A method to quantify the fiber kinematics of planar tissues under biaxial stretch. Journal of Biomechanics 30, 753–756.

Carroll, M., 2011. A strain energy function for vulcanized rubbers. Journal of Elasticity 103, 173–187.

Chagnon, G., Rebouah, M., Favier, D., 2015. Hyperelastic energy densities for soft biological tissues: A review. Journal of Elasticity 120, 129–160.

Crespo, J., Latorre, M., Monáns, F., 2017. WYPIWYG hyperelasticity for isotropic, compressible materials. Computational Mechanics 59, 73–92.

Crespo, J., Montáns, F., 2019. General solution procedures to compute the stored energy density of conservative solids directly from experimental data. International Journal of Engineering Science 141.

Criscione, J., 2003. Rivlin's representation formula is ill-conceived for the determination of response functions via biaxial testing. Journal of Elasticity 70, 129–147.

Doi, M., Edwards, S., 1988. The theory of polymer dynamics. Clarendon Press, Oxford.

Edwards, S., 1967. Statistical mechanics with topological constraints: I. Proceedings of the Physical Society 91, 513–519.

Edwards, S., Vilgis, T., 1988. The tube model theory of rubber elasticity. Reports on Progress in Physics 51, 243–297.

Flory, P., 1969. Statistical Mechanics of Chain Molecules. Interscience, New York.

Flory, P., 1976. Statistical thermodynamics of random entworks. Proceedings of the Royal Society of London, A: Mathematical, Physical and Engineering Sciences 351, 351–380.

Flory, P., Erman, B., 1982. Theory of elasticity polymer networks. 3. Macromolecules 15, 800–806.

Flory, P., Rehner, J.J., 1943. Statistical mechanics of cross-linked polymer networks. The Journal of Chemical Physics 11, 512–520.

Gent, A., 1996. A new constitutive relation for rubber. Rubber Chemistry and Technology 69, 59–61.

Gilbert, T., Sacks, M., Grashow, J., Woo, S.Y., Badylak, S., Chancellor, M., 2006. Fiber kinematics of small intestinal submucosa under biaxial and uniaxial stretch. Journal of Biomechanical Engineering 128, 890–898.

Gusev, A., Schwarz, F., 2019. Molecular dynamics validation and applications of the maximum entropy homogenization procedure for predicting the elastic properties of gaussian polymer networks. Macromolecules 52, 9445–9455.

Hart-Smith, L., 1966. Elasticity parameters for finite deformations of rubber-like materials. Zeitschrift Für Angewandte Mathematik Und Physik ZAMP 17, 608–626.

Heinrich, G., Kaliske, M., Küppel, M., Mark, J., Straube, E., Vilgis, T., 2003. The thermoelasticity of rubberlike materials and related constitutive laws. Journal of Macromolecular Science 40, 87–93.

Holzapfel, G., 2000. Nonlinar Solid Mechanics. A Continuum Approach for Engineering. John Wiley & Sons, Chichester.
Horgan, C., Saccomandi, G., 2002. Constitutive modeling of rubber-like and biological materials with limiting chain extensibility. Mathematics and Mechanics of Solids 7, 353–371.
Horgan, C., Schwartz, J., 2005. Constitutive modeling and the trousers test for fracture of rubber-like materials. Journal of the Mechanics and Physics of Solids 53, 545–564.
James, H., Guth, E., 1943. Theory of the elastic properties of rubber. The Journal of Chemical Physics 11, 455–481.
Kaliske, M., Heinrich, G., 1999. An extended tube-model for rubber elasticity: Statistical-mechanical theory and finite element implementation. Rubber Chemistry and Technology 72, 602–632.
Kawabata, S., Matsuda, M., Tei, K., Kawai, H., 1981. Experimental survey of the strain energy density of isoprene rubber. Macromolecules 14, 154–162.
Kawamura, T., Urayama, K., Kohjiya, S., 2001. Multiaxial deformations of end-linked poly(dimethylsiloxane) networks. 1. phenomenological approach tro strain energy density function. Macromolecules 34, 8252–8260.
Kearsley, E., Zapas, L., 1980. Some methods of measurement of an elastic strain energy function of the Valanis-Landel type. Journal of Rheology 24, 483–500.
Kiêm, V., Itskov, M., 2016. Analytical network-averaging of the tube model: Rubber elasticity. Journal of the Mechanics and Physics of Solids 95, 254–269.
Kroon, M., 2011. An 8-chain model for rubber-like materials accounting for non-affine chain deformations and topological constraints. Journal of Elasticity 102, 99–116.
Kuhn, W., 1934. über die gestalt fadenförmiger moleküle in lösungen. Kolloid-Zeitschrift 59, 208–216.
Kuhn, W., 1936. Beziehungen zwischen molekülgrösse, statistischer molekülgestalt und elastischen eigenschaften hochpolymerer stoffe. Kolloid-Zeitschrift 76.
Kuhn, W., Grün, F., 1942. Beziehungen zwischen elastischen konstanten und dehnungsdoppelbrechung hochelastischer stoffe. Kolloid-Zeitschrift 101, 248–271.
Lang, M., 2017. Relation between cross-link fluctuations and elasticity in entangled polymer networks. Macromolecules 50, 2547–2555.
Latorre, M., De Rosa, E., Montáns, F., 2017a. Understanding the need of the compression branch to characterize hyperelastic materials. International Journal of Non-Linear Mechanics 89, 14–24.
Latorre, M., Montáns, F., 2014. What-You-Prescribe-Is-What-You-Get orthotropic hyperelasticity. Computational Mechanics 53, 1279–1298.
Latorre, M., Peña, E., Montáns, F., 2017b. Determination and finite element validation of the WYPIWYG strain energy of superficial fascia from experimental data. Annals of Biomedical Engineering 45, 799–810.
Lopez-Pamies, O., 2010. A new i_1-based hyperelastic model for rubber elastic materials. Comptes Rendus Mecanique 338, 3–11.
Mark, J., Erman, B., 1988. Rubberlike elasticity: A molecular primer. Wiley, New York.
Markmann, G., Verron, E., 2006. Comparison of hyperelastic models for rubber-like materials. Rubber Chemistry and Technology 79, 835–858.
Menzel, A., Waffenschmidt, T., 2009. A microsphere-based remodelling formulation for anisotropic biological tissues. Philosophical Transactions of the Royal Society A: Mathematical, Physical and Engineering Sciences 367, 3499–3523.
Meyer, K., Susich, G., Valkó, E., 1932. Die elastischen eigenschaften der organischen hochpolymeren und ihre kinetische deutung. Kolloid-Zeitschrift 59, 208–216.
Miehe, C., Göktepe, S., Lulei, F., 2004. A micro-macro approach to rubber-like materials—Part I: the non-affine micro-sphere model of rubber elasticity. Journal of the Mechanics and Physics of Solids 52, 2617–2660.
Mooney, M., 1940. A theory of large elastic deformations. Journal of Applied Physics 11, 582.
Müller, I., Weiss, W., 2005. Entropy and Energy. Springer, Berlin.
Obata, Y., Kawabata, S., Kawai, H., 1970. Mechanical properties of natural rubber vulcanizates in finite deformation. Journal of Polymer Science Part A-2: Polymer Physics 8, 903–919.
Ogden, R., 1972. Large deformation isotropic elasticity: on the correlation of theory and experiment for incompressible rubberlike solids. Proceedings of the Royal Society of London A 326.
Ogden, R., Saccomandi, G., Sgura, I., 2004. Fitting hyperelastic models to experimental data. Computational Mechanics 34, 484–502.
Pancheri, F., Dorfmann, L., 2014. Strain-controlled biaxial tension of natural rubber: new experimental data. Rubber Chemistry and Technology 87, 120–138.
Qin, J., So, J., Milner, S., 2012. ube diameter of stretched and compressed permanently entangled polymers. Macromolecules 45, 9816–9822.
Rivlin, R., 1948. Large elastic deformations of isotropic materials: IV. Further developments of the general theory. Philosophical Transactions of the Royal Society A 241, 379–397.
Rivlin, R., Saunders, D., 1951. Large elastic deformations of isotropic materials VII. Experiments on the deformation of rubber. Philosophical Transactions of the Royal Society A: Mathematical, Physical and Engineering Sciences 243, 251–288.
Romero, X., Latorre, M., Montáns, F., 2017. Determination of the wypiwyg strain energy density of skin through finite element analysis of the experiments on circular specimens. Finite Elements in Analysis and Design 134, 1–15.
Rubinstein, M., Panyukov, S., 1997. Nonaffine deformation and elasticity of polymer networks. Macromolecules 30, 8036–8044.
Sáez, P., V., A., Peña, E., Doblaré, M., Martínez, M., 2012. Anisotropic microsphere-based approach to damage in soft fibered tissue. Biomechanics and Modelling in Mechanobiology 11, 595–608.
Shariff, M., 2000. Strain energy function for filled and unfilled rubberlike material. Rubber Chemistry and Technology 73, 1–18.

Shariff, M., 2017. On the spectral constitutive modelling of transversely isotropic soft tissue: Physical invariants. International Journal of Engineering Science 120, 199–219.
Staudinger, H., 1920. über polymerisation. Berichte der deutschen chemischen Gesellschaft 53, 1073–1985.
Steinmann, P., Hossain, M., Possart, G., 2012. Hyperelastic models for rubber-like materials: consistent tangent operators and suitability for treloar's data. Archive of Applied Mechanics 82, 1183–1217.
Sussman, T., Bathe, K., 2008. A model of incompressible isotropic hyperelastic material behavior using spline interpolations of tension-compression test data. Communications in Numerical Methods in Engineering 25, 53–63.
Treloar, L., 1944. Stress-strain data for vulcanized rubber under various types of deformation. Rubber Chemistry and Technology 17, 813–825.
Treloar, L., 1975. The physics of Rubber Elasticity. Oxford University Press.
Urayama, K., 2006. An experimentalist's view of the physics of rubber elasticity. Journal of Polymer Science 44, 3440–3444.
Valanis, K., Landel, R., 1967. The strain energy function of a hyperelastic material in terms of the extension ratios. Journal of Applied Physics 38, 2997.
Verron, E., Gros, A., 2017. An equal force theory for network models of soft materials with arbitrary molecular weight distribution. Journal of the Mechanics and Physics of Solids 106, 176–190.
Volokh, K., 2016. Mechanics of Soft Materials. Springer, Singapore.
Waffenschmidt, T., Menzel, A., Kuhl, E., 2012. Anisotropic density growth of bone. a computational micro-sphere approach. International Journal of Solids and Structures 49, 1928–1946.
Wall, F., 1942. Statistical thermodynamics of rubber (and part II). The Journal of Chemical Physics 10 (2 and 7), 132–134 and 485–488.
Ward, I., Hadley, D., 1993. An introduction to the mechanical properties of solid polymers. John Wiley & Sons, Chichester.
Wen, Q., Basu, A., Janmey, P., Yodh, A., 2012. Non-affine deformations in polymer hydrogels. Soft Matter 8.
Wu, P., van der Giessen, E., 1992. On improved 3-D non-Gaussian network models for rubber elasticity. Mechanics Research Communications 19.
Wu, P., van der Giessen, E., 1993. On improved network models for rubber elasticity and their applications to orientation hardening in glassy polymers. Journal of the Mechanics and Physics of Solids 41, 427–456.
Xiang, Y., Zhong, D., Wang, P., Mao, G., Yu, H., Qu, S., 2018. A general constitutive model of soft elastomers. Journal of the Mechanics and Physics of Solids 117, 110–122.
Yeoh, O., 1993. Some forms of the strain energy function for rubber. Rubber Chemistry and Technology 66, 754–771.
Yeoh, O., Fleming, P., 1997. A new attempt to reconcile the statistical and phenomenological theories of rubber elasticity. Journal of Polymer Science, Part B: Polymer Physics 35, 1919–1931.